Quaternary Science Reviews 344 (2024) 108959

Contents lists available at ScienceDirect

Quaternary Science Reviews

journal homepage: www.elsevier.com/locate/quascirev

Dynamic landscape response to Younger Dryas and earliest Holocene cooling events in the European Eastern Alps (Austria)

Charlotte Gild-Haselwarter [a], Michael Meyer [b], Clemens Geitner [a], Jean Nicolas Haas [c], Sanja Vranjes-Wessely [b], Clivia Hejny [d], Werner Kofler [c], Karl Krainer [b], Daniel Remias [e], Sönke Szidat [f], Diethard Sanders [b,*]

[a] Institute of Geography, University of Innsbruck, Innrain 52, A-6020, Innsbruck, EU, Austria
[b] Institute of Geology, University of Innsbruck, Innrain 52, A-6020, Innsbruck, EU, Austria
[c] Institute of Botany, University of Innsbruck, Sternwartestraße 15, A-6020, Innsbruck, EU, Austria
[d] Institute of Mineralogy and Petrography, University of Innsbruck, Innrain 52, A-6020, Innsbruck, EU, Austria
[e] Faculty of Natural and Life Sciences, Hellbrunnerstraße 34, A-5020, Salzburg, EU, Austria
[f] Department of Chemistry, Biochemistry and Pharmaceutical Science & Oeschger Centre for Climate Change Research, University of Bern, Freiestrasse 3, CH-3012, Bern, Switzerland

ARTICLE INFO

Keywords:
Quaternary
Loess
Aeolian sediments
Palynology
Luminescence dating
IRSL
OSL
Radiocarbon dating

ABSTRACT

In classic loess areas research into dust deposition and concomitant environmental changes has a long history and numerous well-investigated loess-palaeosol sequences provide insights into Late Quaternary landscape responses to climatic change on orbital to centennial time scales. This contrasts with mountain regions, where an understanding of dust deposition under rapidly changing climatic and environmental conditions is much less developed. Here we describe two sediment records from the Austrian Alps that provide rare evidence for intramontane loess accumulation. Dust deposition has been numerically constrained to the Younger Dryas (YD) to earliest Holocene interval, making these sites the first proof of significant intramontane aeolian activity during this time interval in the Eastern Alps.

At study site 1, located in the Northern Calcareous Alps, a loess layer 10–20 cm in thickness and laterally exposed over more than 300 m is sandwiched into an alluvial-fan succession. Two optically-stimulated luminescence ages of quartz and four radiocarbon ages of charcoals indicate loess accumulation during the Younger Dryas to earliest Holocene. This laterally extensive loess drape suggests much drier climatic conditions compared to today, which is corroborated by palynological investigations. Macro- and micro-charcoal particles within the loess indicate regional wildfires that might have exaggerated climatically induced sedimentary processes. The second site is a Mesolithic site located ~30 km southeast of site 1. At site two, redeposited till and pebbly scree are sharply overlain by a few centimetre thick light-grey loess layer, which is capped by the archaeological living floor hosting ^{14}C dated fireplaces suggesting human presence as early as 10.9 ± 0.2 cal ka BP. These radiocarbon ages in combination with single-grain IRSL dating of feldspar at site two suggests concomitant aeolian deposition at site 1 and 2.

Recently, a widespread drape of loess deposited immediately subsequent to the LGM was described for the same sector of the Eastern Alps (Gild et al., 2018). The present study expands on these findings and provides evidence for the recurrence of loess deposition also during the YD to earliest Holocene, and suggests a highly sensitive response of the geomorphic system in mountain ranges to abrupt post-LGM climate fluctuations. We conclude that, in addition to moraine records of Alpine glaciers and speleothems that accurately chronicle Late Glacial temperature fluctuations, the spatio-temporal pattern of inner-Alpine loess deposits records the mode and sensitivity of landscape responses to such cooling events. Because such aeolian sediment layers can be redeposited or pedologically overprinted, they are often overlooked, and are thus still severely under-researched.

* Corresponding author.
E-mail address: Diethard.Sanders@aon.at (D. Sanders).

https://doi.org/10.1016/j.quascirev.2024.108959
Received 4 June 2024; Received in revised form 4 September 2024; Accepted 8 September 2024
Available online 20 September 2024

1. Introduction

Deposition of airborne mineral dust is an important process during the Quaternary, because aeolian processes are sensitively responding to climatic and environmental changes, yet they are also capable of partly driving these very changes (Shao et al., 2011; Muhs, 2013; Knippertz and Stuut, 2014; Újvári et al., 2017; Zhao et al., 2022). In order to investigate aeolian dynamics, researchers traditionally turned to terrestrial archives such as the exceptionally thick loess-palaeosol sequences of the Chinese loess plateau (e.g., Liu, 1965, 1985; Heller and Liu, 1982; Kohfeld and Harrison, 2001; Stevens et al., 2018), the loess-palaeosol sequences in the forelands of the Alpine-Carpathian belt (e.g., Fink and Kukla, 1977; Forno, 1979; Cremaschi, 1990; Frechen et al., 2003; Thiel et al., 2011, b; Terhorst et al., 2014; Nigst et al., 2014; Fenn et al., 2022) or to the vast high-altitude plains of the Andean Altiplano and the Tibetan Plateau and their aeolian sediments (e.g., Lehmkuhl et al., 2000; Zárate, 2003; Klinge and Lehmkuhl, 2015; Li et al., 2020). While research into dust deposition and concomitant climatic change has a long history in these classic loess areas, the understanding of dust-climate interactions in mountains and intramontane settings is much less advanced, partly due to the following reasons: (i) in many mountain ranges aeolian dust deposition is often not confined to glacial periods, because ice-stream networks or valley glaciers were occupying much of the mountain ranges during full glaciations and (ii) erosion is typically intense in high relief mountainous settings, destroying any terrestrial aeolian traces or leaving only a thin and extremely patchy aeolian sediment drape compared to lowlands and wide plateaus, where more extensive and thicker loess sequences and sand sheets accumulate (McGowan, 1997; Bäumler, 2001; Caspari et al., 2009; Smalley et al., 2009; Munroe et al., 2015). Furthermore, in mountain ranges, aeolian input can be crucial to sustain biological productivity in mountain lakes (Ballantyne et al., 2011; Bigelow et al., 2020) as well as for the development of soils (Reynolds et al., 2001; Küfmann, 2003; Muhs and Benedict, 2006; Lawrence et al., 2011; Grashey-Jansen et al., 2014; Munroe et al., 2020). Hence, loess and/or aeolian dust stored in alpine sediment archives including soils are important environmental indicators bearing significant potential for reconstructing paleoclimatic change and associated landscape responses. However, aeolian processes in alpine regions are still relatively poorly understood (Sticher et al., 1975; McGowan and Sturman, 1997; Küfmann, 2003; Martignier et al., 2015; Wolfe and Lian, 2021).

In the context of the European Alps, Kravogl (1873) and Blaas (1885) first mentioned inner-Alpine aeolian layers in the wider Innsbruck area and the Northern Calcareous Alps (NCA), Austria (Fig. 1A) and concluded that these types of intramontane sediments merit further investigation. These aeolian layers are composed of silt-sized grains of quartz, feldspars, phyllosilicates and, more rarely, of calcite and/or dolomite and, in the NCA, give rise to Cambisol soils (Gild et al., 2018).

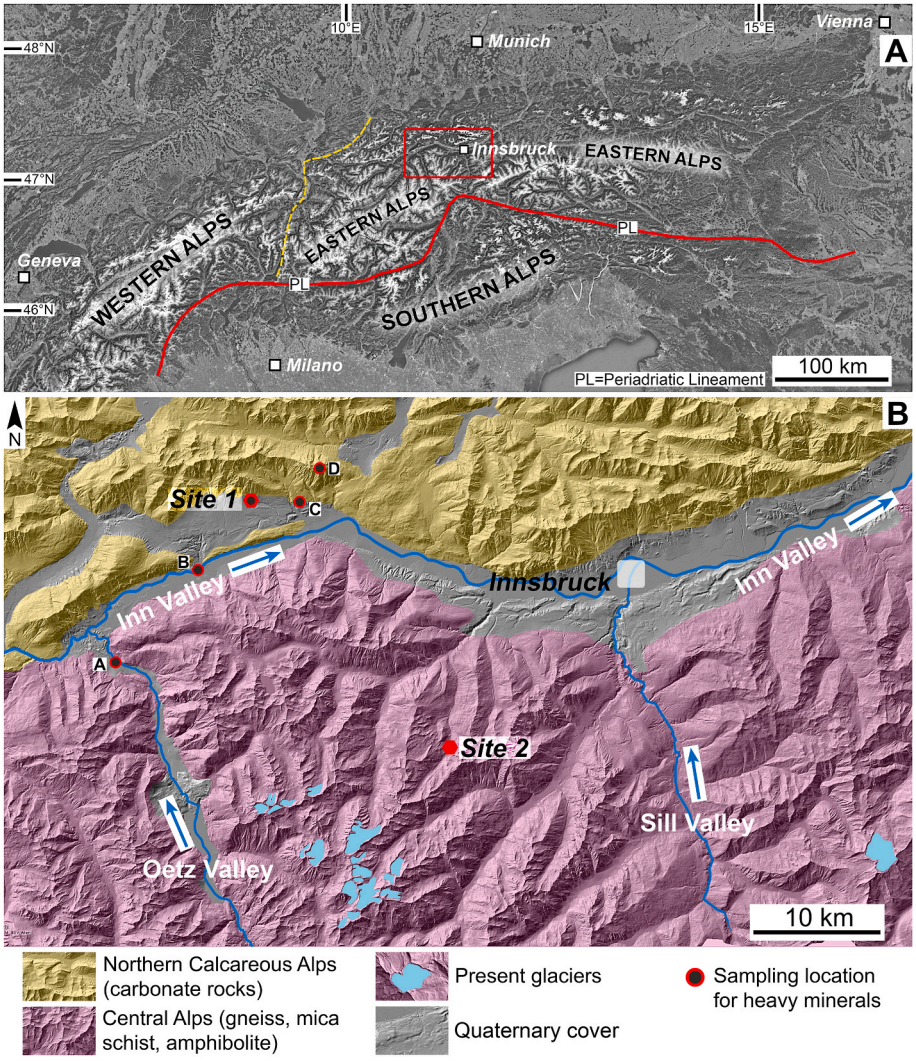

Fig. 1. A) Location of the investigation area (red rectangle, compare Fig. 1B) within the Eastern European Alps. B) Regional geology and location of sites 1 and 2. Letters A to D indicate sampling locations for heavy mineral spectra, arrows indicate flow directions of main rivers.

Pedological studies concluded that the Cambisols of the NCA of polymictic silt might result from aeolian deposition, and that aeolian input presumably occurred sometime during the Late Glacial (Blockley et al., 2012; Küfmann, 2003). Veit et al. (2002), investigating periglacial cover beds containing polymictic silt in several regions in the Alps (e.g., Hohe Tauern, Valais), came up with a similar conclusion; i.e., that aeolian sediments within the subalpine and montane zones should be attributed to the Late Glacial, while above the tree line, aeolian deposits may accumulate until present. None of these pedological studies involved numerical dating to accurately pinpoint the age of loess deposition. Gild et al. (2018) were the first who provided optically-stimulated luminescence (OSL) ages for these deposits in the Eastern Alps. Their quartz OSL chronology suggests that a laterally extensive loess drape accumulated early after the Last Glacial Maximum (LGM; Gild et al., 2018; Sanders et al., 2018).

In the European Alps, environmental processes relevant during the Late Glacial or the Holocene are recorded in lake sediments, peat bogs, speleothems or via moraine successions (e.g., Boch et al., 2009; Ivy-Ochs et al., 2009; Ilyashuk et al., 2009; Koltai et al., 2018). Yet, so far, with very few late Holocene exceptions (Grüger and Jerz, 2010), no securely dated aeolian sediment successions from these time intervals have been reported for the Eastern Alps.

Here we describe layers of polymictic silt interpreted as loess from two sites in the Eastern Alps (Fig. 1B). The loess layers were dated via luminescence and radiocarbon. We show that each layer accumulated at the turn from the Younger Dryas to the earliest Holocene. This is the first numerically constrained documentation that in the Eastern Alps loess accumulation was not confined to a single early Late Glacial phase (Gild et al., 2018), but occurred repeatedly after the LGM. Our results also suggest that such loess layers can serve as dateable marker horizons that highlight Late Glacial to early Holocene dynamics of intramontane sediment cascades.

2. Quaternary geological setting and morphodynamics of the investigation area

The Eastern Alps are a W-E striking mountain range of basement- and cover-thrust nappes revealing metamorphic basement nappes south of the Inn Valley (the Central Alps) and non-metamorphic cover nappes composed of shallow-water carbonates (the Northern Calcareous Alps; NCA), north of the Inn Valley (Oberhauser, 1980; Handy et al., 2015). As such the Inn Valley represents a major tectonic lineament and is also one of the longest alpine longitudinal valleys. Site 1 is located in the Inn Valley at the southern rim of the NCA, site 2 is located within the metamorphic basement ~25 km southeast of site 1 in the Central Alps in a tributary to the Inn Valley (Fig. 1).

During the regional LGM (ca. 26–21 ka BP), the Eastern Alps, and thus site 1 and 2, were covered by an ice stream network surmounted by nunataks (Van Husen and Reitner, 2011). Subsequent to ca. 21 ka BP the LGM ice extent was reduced by roughly 50% within a few millennia, leaving the major alpine valleys, including the Inn Valley, deglaciated by ca. 18.5–18 ka (Fig. 2) (Patzelt and Resch, 1986; Van Husen and Reitner, 2011; Patzelt, 2014). During this early deglacial phase a regional drape of intramontane loess accumulated directly on this freshly deglaciated landscape, including ice-free slopes and saddles adjacent to nunataks (Gild et al., 2018).

During Heinrich Event 1 (17.1–14.3 ka; Hodell et al., 2017), alpine valley glaciers re-advanced, depositing the so-called Gschnitz stadial moraines in many alpine valleys, dating to ca. 15.4 ka BP; (Ivy Ochs et al., 2005, 2008, Fig. 2). The Gschnitz re-advance was restricted to the upper reaches of the alpine longitudinal valleys and to major tributaries. Hence, site 1 located in the middle stretches of the Inn Valley remained ice-free, while site 2 was covered by the local Gschnitz valley glacier (Kerschner, 2011).

The first significant Late Glacial warming occurred ca. 14.7–12.8 ka ago with the Bølling-Allerød interstadial (Ilyashuk et al., 2009;

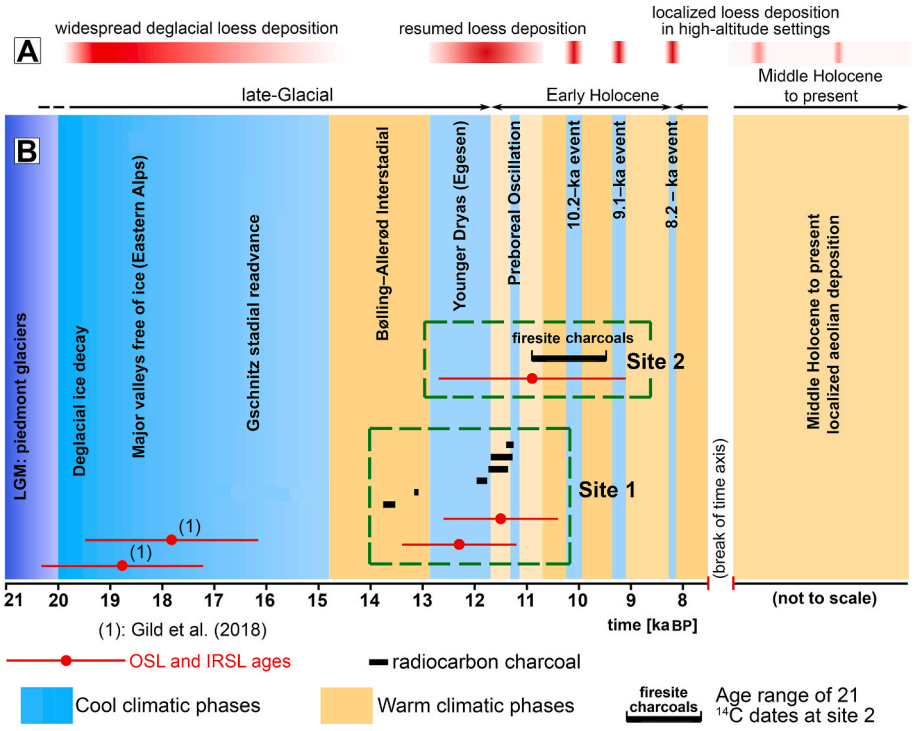

Fig. 2. Late Glacial to Holocene climate history (b) and conceptualization of concomitant aeolian dynamics (a) in the Eastern Alps. The phases of aeolian deposition (red bars in a) are numerically constrained for the early deglacial loess deposits by Gild et al. (2018) and for the loess deposits of the Younger Dryas and the Preboreal Oscillation via this study. The phases of localized loess deposition in high-altitude settings during subsequent Early Holocene cold phases (i.e. during the 10.2, 9.1 and 8.2 ka events) as well as during the Middle Holocene are not numerically dated (yet) but suggested on conceptual climatic-sedimentary grounds only. See text for further details.

Lauterbach et al., 2011, Fig. 2), followed by the Younger Dryas (YD) cooling event lasting from ca. 12.8 to 11.7 ka BP (Reinig et al., 2021). In the Alps, the YD was associated with a lowering of the mean annual air temperature by ~3.5–6 °C (Lotter et al., 2000; Ilyashuk et al., 2009), and advancing valley glaciers that halted several kilometres upstream of the Gschnitz terminal moraines (Kerschner et al., 2000; Ivy-Ochs et al., 2006, 2009; Ivy-Ochs, 2015; Bichler et al., 2016; Moran et al., 2016a). During the YD site 2 was situated in the immediate fore field of the local YD glacier (Figs. 1 and 4). No YD glacial features exist in the local catchment that nourished the debris fan on which site 1 is situated (Figs. 1 and 3).

Some geomorphological and geochronological studies suggest that alpine catchments reacted to smaller cold oscillations that occurred subsequent to the YD (such as the Preboreal oscillation at ca. 11.3 ka; Fisher et al., 2002; Bos et al., 2007) via minor glacier re-advances and enhanced rock glacier activity, while the 9.1 or 8.2 ka events left no

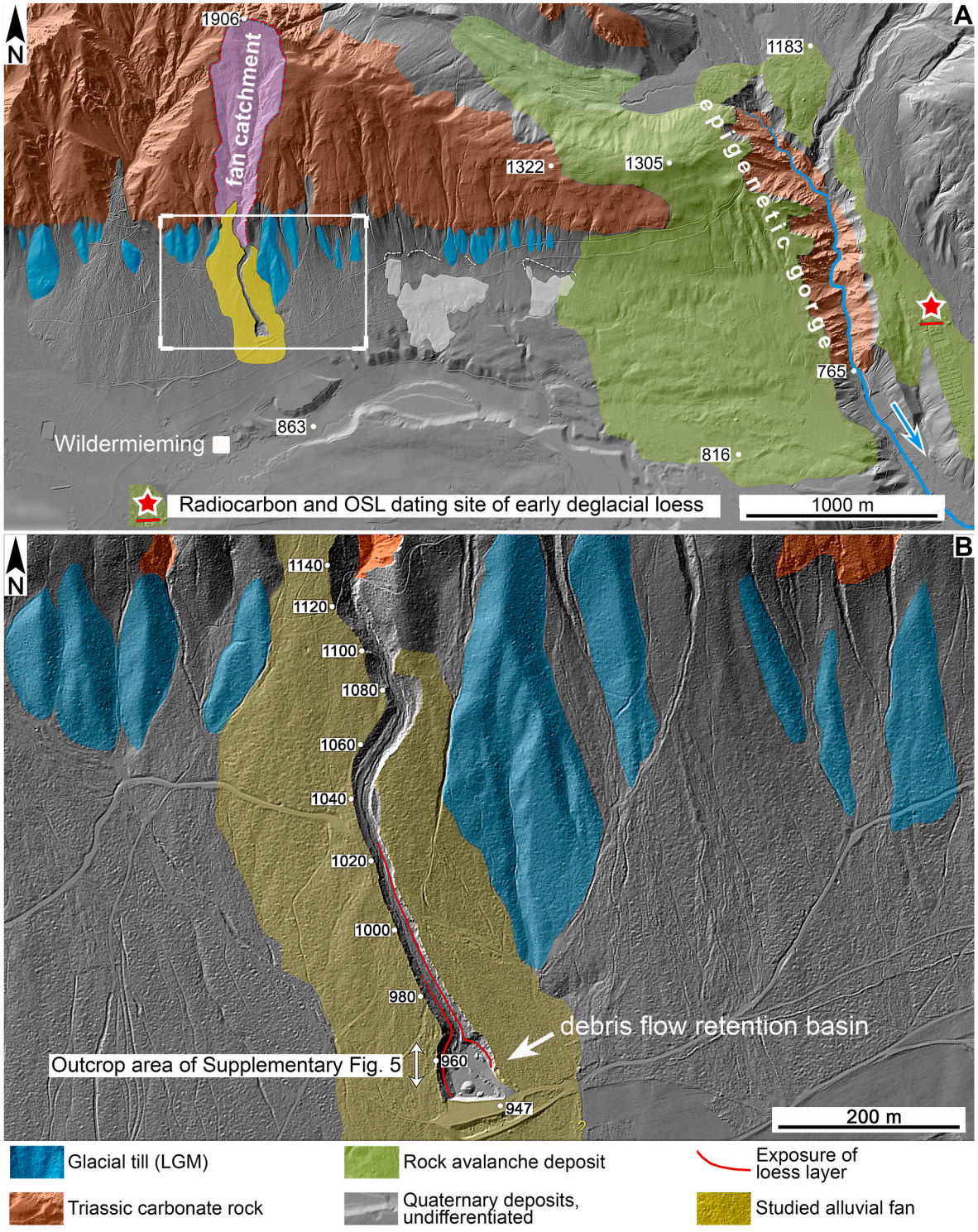

Fig. 3. A) Overview map of site 1 (Wildermieming) showing alluvial fan containing the loess layer. B) Detailed view of alluvial fan with lateral extension of loess layer marked as red line. Note artificial debris-flow retention basin that was dredged in the 1970ies and is responsible for the retrograde incision into the alluvial fan succession that occurred since then.

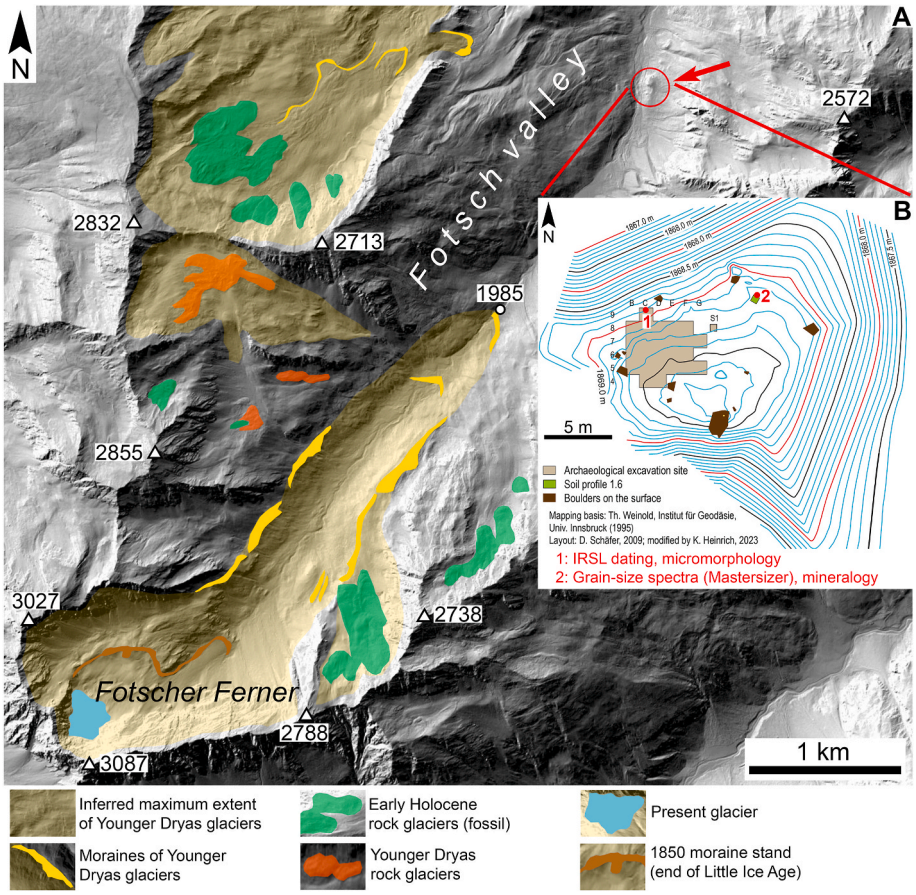

Fig. 4. A) Overview map of the upper Fotsch valley and location of site 2 (Ullafelsen, red arrow), as well as former extent of local valley glaciers and rock glaciers; simplified from Kerschner (2011). B) Ullafelsen site map (adapted from Schäfer, 2011b) showing archaeological excavation area and location of further excavation pits (soil sections). The location of the IRSL sample for direct dating of the site 2 loess layer is marked with a red arrow, the radiocarbon samples were retrieved from the entire archaeological excavation area.

conclusive morphological imprint in the same catchments (Ivy-Ochs et al., 2006; Kerschner and Ivy-Ochs, 2008; Ivy-Ochs, 2015; Krainer et al., 2015; Moran et al., 2016a, b; Fig. 2). At site 1 and 2 no glacier or rock glacier deposits have been identified that could be unequivocally attributed to these smaller cold events occurring subsequent to the YD.

As one of the largest longitudinal valleys in the Eastern Alps the Inn Valley, which is also hosting site 1, contains a thick succession of Quaternary deposits (Fig. 1B). These deposits accumulated in response to Pleistocene as well as Holocene climatic forcings and include sediments that document the process of LGM ice-build up and decay. The sedimentary infill of the Inn Valley attains a thickness of several hundred meters, as documented from e.g. drill cores, geophysical investigations and rare outcrops (Patzelt and Resch, 1986; Starnberger et al., 2013; Barrett et al., 2017). Yet, despite their thickness, these valley-fill deposits and their climatic significance are only poorly understood, because many of these deposits lack numerical age control and are often not directly accessible. Yet, for the Late Glacial and the Holocene a pattern of fluvial aggradation and incision is apparent in the sedimentary record of the Inn Valley that is discussed in more detail with respect to the aeolian dynamics recognized at site 1 and 2 in section 6.5.

3. Study sites

The loess layer of study site 1 (47.324625 N, 11.009590 E) (Fig. 1B) is located close to the village Wildermieming in the NCA, and is intercalated into an alluvial fan succession which is part of an array of alluvial fans that onlap a rock slope of Upper Triassic dolostone (Fig. 3). Most of these fans today are abandoned and covered with pine forest up to their apex. The surface sediment of these fans ranges from pebbly deposits composed of dolostone clasts derived from the upslope mountain flank to mixtures of dolostones with sand-to pebble-sized clasts of metamorphic rocks derived from redeposition of LGM glacial drift. The fans are laterally separated by slope facets (Fig. 3).

Aerial photographs of 1946 indicate that the medial to distal part of the studied alluvial fan remained active and aggraded till present. To ban the hazard of debris flows encroaching into the adjacent farmland, a retention basin was excavated in the 1970s, and since then the feeder channel progressively incised to its present depth (Fig. 3B). Today, the alluvial-fan succession is exposed over a maximum incised depth of ~23 m. Within the succession, a yellowish layer of polymictic silt – the loess layer of this study – is clearly identifiable, and can be laterally followed over more than 300 m (Fig. 3B).

Study site 2 (47.147275 N, 11.214949 E; 1869 m a.s.l.) is positioned on the orographically right flank of the upper Fotsch Valley in the Oetztal-Stubai massif of the central Alps (Fig. 1). The Oetztal-Stubai massif is composed of biotite-bearing gneisses and orthogneisses with intercalated lenses of amphibolite and hornblende schists; site 2 is underlain by a biotite-plagioclase gneiss (Hammer, 1929; Nittel, 2011).

Site 2 is situated on top of an elevated, whaleback-like bedrock ledge ~60 m above the valley thalweg and ~6 m above and 30 m ahead of the toe of a local scree slope that confines the valley to the east. This scree slope is ~100 m in vertical extent and currently vegetated (Fig. 4). The rock ledge provided a settling ground for Mesolithic hunter-gatherers; the archaeological site was excavated from 1994 to 2004 and termed Ullafelsen (Fig. 4B) (Schäfer, 2011a; Schäfer et al., 2016). The excavation also exposed the layer of polymictic silt described below and was

already interpreted as an aeolian deposit with a presumptive YD or Early Holocene age by Geitner et al. (2011). The loess layer (dubbed 'light layer' by the archaeologists) was the living floor of these Mesolithic hunter-gatherers, and is scattered with fireplaces and stone artefacts (Schäfer, 2011a). The charcoals record four phases of human settlement that, together, span a maximum time range from 10.9 ± 0.2 to 9.5 ± 0.05 cal ka BP (Table 2).

4. Methods

The methods used in this study are outlined below. Further technical details are available in the electronic supplementary material (ESM).

Sedimentary logs were compiled as well as samples obtained (i) along a ~300 m long laterally continuous outcrop at site 1 (Wildermieming; Fig. 3B) and (ii) from multiple excavation pits at site 2 (Ullafelsen) spread out over an area of 10 × 10 m, where identical soil profiles were encountered in each of these excavation pits (Fig. 4B).

Field mapping was aided by LIDAR images with 1 m ground resolution. Grain size classes are designated according to the Wentworth (1922) scale. Undisturbed thin section samples were extracted from both sites and impregnated with epoxy resin for microscopic thin section analysis under transmitted-light and dark-field illumination using an Olympus SX10 microscope. The designation of sediment fabrics follows the terminology outlined in Stoops (2003) and Stoops et al. (2010).

The grain-size distribution of fine-grained sediments in the 0.02–2000 μm range was determined by laser diffraction via a Malvern Mastersizer 2000® or 3000®, respectively.

The bulk mineralogical composition of loess samples was analysed by standard X-ray powder diffractometry using a Bruker-AXS D8 diffractometer and qualitative and quantitative phase identification was done with the programs DIFFRAC PLUS and TOPAS, respectively.

For provenance analysis heavy mineral spectra were determined according to Boenigk (1983) and Mange and Maurer (1992) from the studied loess layers and compared with heavy mineral spectra from potential alpine source areas.

The shape and surface morphology of sediment grains of selected loess samples were investigated by backscattered electron microscopy using a Digital Scanning Microscope JEOL JSM-5130LV.

A drill core of the loess layer from site 1 was retrieved for high-resolution XRF scanning to check for eventual microscopic or sub-microscopic and chemical layering. Core scanning was done with an Itrax-XRF core scanner (CS-45) and a downcore resolution was 200 μm at an image width of 2 cm. Nine samples taken in regular intervals along the XRF core were analysed for their carbonate content by dissolving pre-weighted samples with 25% hydrochloric acid and determining their weight loss on digestion.

At site 1, two samples each 1 cm^3 in volume were extracted from the loess layer for their palynomorph content: sample WIM-PP-1 from 1 cm below the top and sample WIM-PP-2 from the very base of the loess layer. The samples were prepared following palynological standard procedures (Seiwald, 1980). To quantify palynomorph concentrations a known number of *Lycopodium clavatum* spores were added to each sample as counting standard (Stockmarr, 1971) and a Zeiss Axioscope Lab.A1 microscope was used for analysis.

In total, three samples were taken for luminescence dating: samples WIM 1 and WIM 11 from site 1 and sample UF-1 from site 2. Samples were obtained by hammering stainless steel tubes into freshly cleaned outcrops. At site 1, fine-grained quartz (4–11 μm) was extracted following standard procedures (Wintle, 1997) and, after the successful completion of dose recovery tests, measured as large aliquots via blue light stimulation using the SAR protocol (Murray and Wintle, 2000). Dose rates for site 1 were obtained via a combination of beta and thick-source alpha counting and *in-situ* gamma spectrometry, in order to capture the spatial heterogeneity of the gamma sphere at each sampling point (Bøtter-Jensen and Mejdahl, 1988; Guerin and Mercier, 2011; compare ESM_Luminescence dating).

At site 2, previous OSL tests on quartz extracts yielded blue stimulated luminescence signals that were not suitable for age dating. Hence, coarse feldspar grains (180–212 μm) were extracted from sample UF-1 (Wintle, 1997). Electron microprobe analysis (JEOL Superprobe 8100) of individual feldspar grains revealed that these feldspar extracts were composed of sodium feldspar only. Compared to potassium feldspar, sodium feldspars display lower signal intensities in the blue detection window upon infra-red stimulation (IR), but also reveal lower fading rates and have previously been shown to function as reliable natural dosimeters (Huntley et al., 2007; Barré and Lamothe, 2010; Sohbati et al., 2013; Balescu et al., 2015). The blue emissions of sodium feldspars from sample UF-1 were thus measured on the single-grain level via IR laser stimulation using a SAR-based post-IR IRSL protocol and standard acceptance criteria (Murray and Wintle, 2000; Thomsen et al., 2008; Buylaert et al. 2012). Dose recovery tests and fading tests were conducted, and residual dose values quantified, and the single-grain De distributions analysed using the central age model and the finite mixture model. The dose rate for sample UF-1 was determined via a combination of beta and thick source alpha counting. Because sample UF-1 was taken from ~12 cm depth, the truncated gamma sphere has been considered when calculating the total external dose rate for this sample. The dose rates, De values and resulting burial ages for all samples (WIM 1 and WIM 11 and UF-2) are given in Table 1.

AMS radiocarbon dating at site 1 was done at the Beta Analytic laboratory (lab code: Beta) and the LARA laboratory at the University of Bern (lab code: BE; Szidat et al., 2014). All radiocarbon ages were calibrated with the IntCal20 (Reimer et al., 2020) calibration curve, version OxCal v4.4.2. and reported in Table 2, together with the recalibrated radiocarbon ages from site 2 and other important sites mentioned in the text.

5. Results

5.1. Site 1 Wildermieming: Sedimentary succession

At site 1, the loess layer is exposed over a distance of more than 300 m and is intercalated into an alluvial fan succession that is composed of debris flow and sheet flow deposits (Fig. 3B and ESM Fig. 5). From bottom to top the fan succession can be subdivided into 6 sedimentary units (A to F; ESM Fig. 5, ESM Tables 1 and 2): Unit A comprises clast-supported, extremely poorly sorted cobbly-bouldery debris flow deposits (ESM Fig. 6A). Unit B is a stack of parallel to divergent bedsets of moderately to well-sorted pebbles representing sheet flow deposits (ESM Figs. 5 and 6B). Unit B is capped by an erosional surface followed by another debris flow unit (unit C), which in turn is overlain by the afore mentioned loess layer (unit D; SEM Figs. 5 and 6C). The loess layer drapes the erosional relief, but upstream the base of the loess layer is planar with only minor undulations (ESM Fig. 6D). The loess unit D is sharply overlain by unit E (a parallel-stratified to unstratified poorly sorted interval of debris flow deposits) followed by unit F (parallel-stratified moderately to well-sorted sheet flow deposits; ESM Fig. 6E). The clast fractions of units A to C are composed of dolostone from the local bedrock and contain a few erratic pebbles of metamorphic rocks, while the clast fractions of units E and F comprise local dolostone only.

5.2. Site 1: Sedimentary characteristics of the loess layer

The loess layer consists of fine to coarse-grained silt (Fig. 6A) and over the entire lateral ~300 m of exposure the layer is remarkably constant with respect to thickness, grain size distribution and mineralogical composition. Both the base and the top of the layer are well-defined relative to the under- and overlying debris and sheet flow deposits (Fig. 5A–D). A few isolated pebbles to cobbles of dolostone project into the loess layer or are embedded within it (Fig. 5B and D). Rarely, lenses of fine-to medium-grained dolostone pebbles are intercalated into the silt layer (Fig. 5C). The bulk mineralogical constituents include

Table 1
Dose rates, De values and quartz (Q) OSL ages (obtained via the SAR protocol) and single-grain IRSL ages on sodium feldspar (Na Fsp; obtained via the post-IR IRSL 225 protocol) of the loess sites at Wildermieming (WM; site 1) and Ullafelsen (UF; site 2). Further details see electronic supplementary material (ESM).

Sample	Mineral & grain size (μm)	Alpha dose rate (Gy.ka-1)	Beta dose rate (Gy.ka-1)	Gamma dose rate (Gy.ka-1)	Cosmic dose rate (Gy.ka-1)	Total dose rate (Gy.ka-1)	Aliquots[a] accepted (n)	OD (%)	De (Gy)	Age (ka)[b]
WM_1	Q 4-11	1.15 ± 0.29	2.03 ± 0.20	0.66 ± 0.07	0.08 ± 0.01	3.92 ± 0.36	20	15	45.0 ± 1.6	11.5 ± 1.1
WM_11	Q 4-11	1.15 ± 0.29	2.03 ± 0.20	0.66 ± 0.07	0.07 ± 0.01	3.92 ± 0.36	20	0	48.3 ± 0.6	12.3 ± 1.1
UF-1	Na Fsp 180-212	0.13 ± 0.03	2.05 ± 0.08	0.99 ± 0.04	0.36 ± 0.46	3.54 ± 0.10	27	15	45.0 ± 1.6	11.6 ± 2.1

[a] in the case of sample UF-1 (measured on the single-grain level) one aliquot refers to an individual grain.
[b] ages reported with their 1 sigma uncertainty.

Table 2
AMS Radiocarbon ages of charred wood embedded in the loess layer of site 1 (this study) and atop of the loess layer of site 2 (Schäfer et al., 2011b). All ages are calibrated via IntCal20 (Reimer et al., 2020).

Location	Sample	conventional radiocarbon age (ka BP ± 2σ err)	calibrated radiocarbon age (cal. ka BP ± 2σ err)	Reference	Notes
Site 1 (Wieldermieming)	A (WIM_2020_HK_2b)	11.78 ± 0.062	13.64 ± 0.048	this study	Large Pinus cembra fragment, stuck in unit C projecting into loess layer, probably a remanent tree root
Site 1 (Wieldermieming)	B (WIM 1)	10.04 ± 0.06	11.55 ± 0.078	this study	Upper part of loess layer
Site 1 (Wieldermieming)	C (WIM 2)	10.21 ± 0.06	11.87 ± 0.042	this study	Upper part of loess layer
Site 1 (Wieldermieming)	D (WIM 3)	11.19 ± 0.06	13.13 ± 0.016	this study	Upper part of loess layer; this charcoal sample probably reworked from older deposits
Site 1 (Wieldermieming)	E (WIM 7)	9.99 ± 0.06	11.48 ± 0.084	this study	Upper part of loess layer
Site 1 (Wieldermieming)	F (WIM_2020_HK_3)	9.91 ± 0.052	11.32 ± 0.032	this study	Bulk age of 50 charred larch/spruce type wood pieces; topmost part of loess layer
Site 2 (Ullafelsen)	a	8.66 ± 0.05	9.65 ± 0.23	Schäfer (2011b)	
Site 2 (Ullafelsen)	b	8.77 ± 0.08	9.85 ± 0.597	Schäfer (2011b)	
Site 2 (Ullafelsen)	c	9.24 ± 0.04	10.41 ± 0.299	Schäfer (2011b)	
Site 2 (Ullafelsen)	d	9.3 ± 0.045	10.47 ± 0.354	Schäfer (2011b)	
Site 2 (Ullafelsen)	e	9.33 ± 0.04	10.55 ± 0.273	Schäfer (2011b)	
Site 2 (Ullafelsen)	f	9.35 ± 0.04	10.56 ± 0.26	Schäfer (2011b)	
Site 2 (Ullafelsen)	g	9.36 ± 0.04	10.56 ± 0.262	Schäfer (2011b)	
Site 2 (Ullafelsen)	h	9.38 ± 0.045	10.59 ± 0.289	Schäfer (2011b)	
Site 2 (Ullafelsen)	i	9.46 ± 0.04	10.82 ± 0.488	Schäfer (2011b)	
Site 2 (Ullafelsen)	k	9.51 ± 0.04	10.83 ± 0.477	Schäfer (2011b)	
Site 2 (Ullafelsen)	l	9.52 ± 0.055	10.84 ± 0.495	Schäfer (2011b)	
Site 2 (Ullafelsen)	m	9.54 ± 0.08	10.88 ± 0.57	Schäfer (2011b)	
Site 2 (Ullafelsen)	n	9.54 ± 0.04	10.89 ± 0.39	Schäfer (2011b)	
Site 2 (Ullafelsen)	o	9.58 ± 0.04	10.94 ± 0.405	Schäfer (2011b)	
Site 2 (Ullafelsen)	p	9.5 ± 0.05	10.83 ± 0.492	Schäfer (2011b)	
Site 2 (Ullafelsen)	q	9.4 ± 0.05	10.6 ± 0.314	Schäfer (2011b)	
Site 2 (Ullafelsen)	r	9.53 ± 0.05	10.88 ± 0.436	Schäfer (2011b)	
Site 2 (Ullafelsen)	s	9.4 ± 0.05	10.6 ± 0.314	Schäfer (2011b)	
Site 2 (Ullafelsen)	t	9.53 ± 0.05	10.88 ± 0.436	Schäfer (2011b)	
Site 2 (Ullafelsen)	u	3.03 ± 0.04	3.22 ± 0.28	Schäfer (2011b)	outlier, not used for weighted grande mean age calculation of loess layer at site 2
Site 2 (Ullafelsen)	v	8.65 ± 0.05	9.64 ± 0.222	Schäfer (2011b)	
Site 2 (Ullafelsen)	w	8.52 ± 0.05	9.5 ± 0.104	Schäfer (2011b)	
Site Zugspitzplatt		7.42 ± 0.06	8.26 ± 0.158	Grüger and Jerz (2010)	Organic sample from a doline aolian infill
Site Innsbruck-Klinik		12.72 ± 0.08	15.16 ± 0.278	Patzelt and Weber (2015)	

quartz, phyllosilicates (chlorite, muscovite), feldspar and highly variable amounts of dolomite derived from erosion of the local dolostone bedrock (Fig. 6B). The heavy mineral spectrum of the silt layer is characterized by high amounts of amphibole, garnet and opaque minerals, while epidote, apatite and staurolite are minor constituents (Fig. 7).

To identify a potential layering not obvious with the naked eye we applied thin section petrography in tandem with XRF scanning on a 9.5 cm diameter core that covered the entire loess layer. The results show that across its entire thickness, the loess layer is a well-sorted polymictic silt (Fig. 8). Microscopically faint latisepic to turbate fabric indicated by mica flakes is evident (Fig. 5E and F). Over most of its vertical extent, the core displays fairly constant counts of Si, K, Fe (proxies for silicate minerals) and of Ca (proxy for carbonate minerals) (Fig. 8), except for the topmost 1.5 cm where Si, K and Fe decline and Ca increases. Macroscopically these topmost 1.5 cm display a mottled fabric caused by alternating patches of pure siliciclastic silt with patches enriched in sand-sized dolostone clasts. No evidence for a layering, a break in sedimentation or intermittent erosion were identified in the XRF scan or under the microscope.

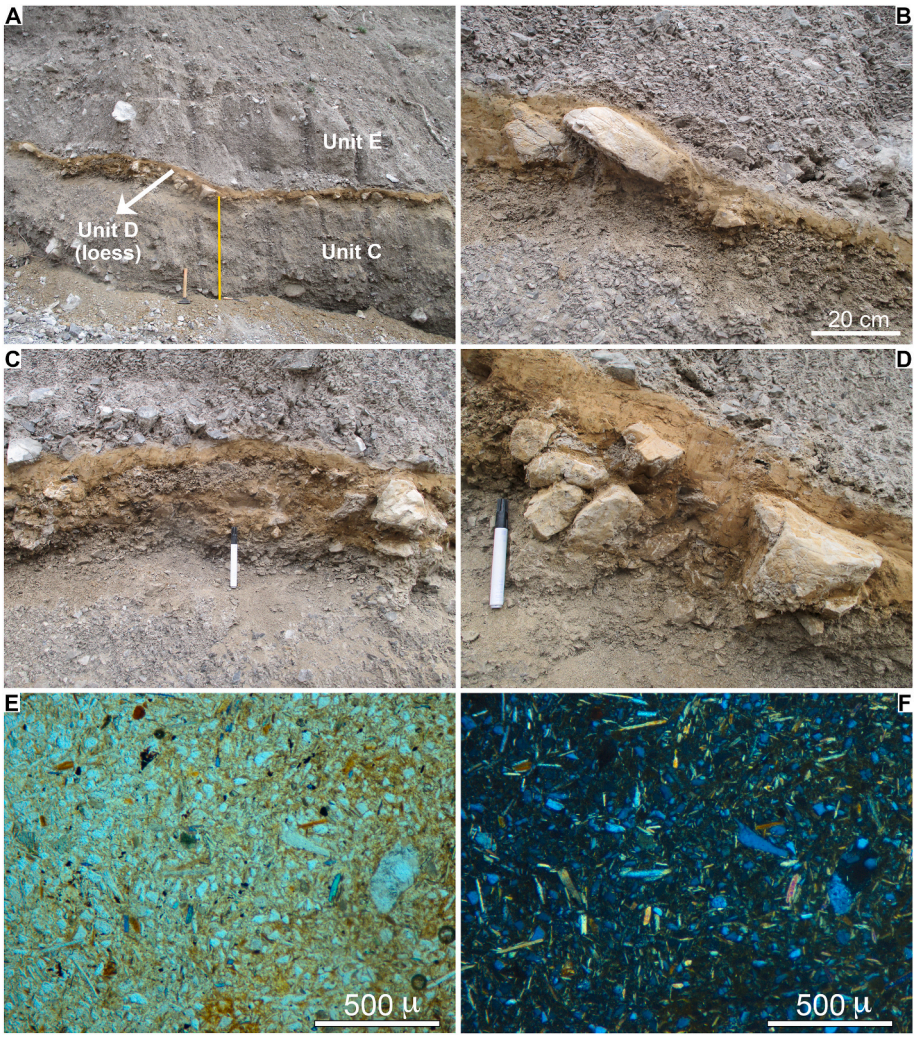

Fig. 5. Sedimentary details of the alluvial fan succession and intercalated loess layer at site 1 (Wildermieming). A) Outcrop image of the loess layer (unit D) at 970 m a.s.l. imbedded between the debris flow units C and E. Yellow scale bar is 1 m. In images A to D upslope is to the left hand-side. B) Closeup of A showing two cobbles of Triassic dolostone embedded within the loess layer. Note upslope imbrication of the cobbles and pinch and swell structures of the loess layer. C) Closeup of A showing thin lens of dolostone scree and pebbles (outlined by stipples) intercalated into the loess layer. Pen: 14 cm. D) Closeup of A showing coarse pebbles to small cobbles of Triassic dolostone loosely scattered along the boundary between units C and D and draping of the loess layer. Pen: 14 cm. E and F) Thin sections of loess layer und parallel nicols (E) and crossed nicols (F). Note turbate fabric highlighted by platy constituents (mainly micas) and by variations in brownish humic substance.

5.3. Site 1: Macro- and microscopic organic content

Macro- and microscopic charcoal fragments are common in the loess layer. Larger pieces of charred wood are concentrated at the base and in the upper part or on top of the loess layer (Fig. 9C), but smaller charcoal pieces are also floating within the matrix. Also, a well-preserved charred piece of *Pinus cembra* (Swiss stone pine) ~10 cm in size and comprising 20 tree rings stuck within the underlying debris flow unit (interval C) and projecting into the loess layer, was observed (Fig. 9A and B; sample A in Table 2). This piece of pinus cembra is interpreted as situ root. Charred conifer needles (probably *Pinus*) are often encountered in freshly broken pieces of loess (Fig. 9D). Determination of 50 pieces of macroscopic charcoal revealed that they pertain either to *Larix decidua or Picea abies*, but could not be clearly assigned due to their charred state. Furthermore, microscopically charred pieces of conifer wood were fairly common in the loess layer and rarely Pinaceae microsporophyll (a stamen, probably *Pinus*) were encountered too (Fig. 9D, E and 9F).

The two palynological samples are characterized by low pollen concentrations, but both samples contained abundant microscopic charcoal (>5000 per 1 cm^3 of sediment; **ESM** Table 3). Based on these two samples the pollen spectrum of the loess layer is characterized by tree pollen from alder (*Alnus*), birch (*Betula*), and undifferentiated pine species (*Pinus*). Furthermore, pollen of Poaceae (>37 µm) and Cyperaceae grasses of *Thalictrum* (meadow-rue) were present. Ancillary spores of mosses (including *Entosthodon hungaricus*) and fungi were encountered too. In sample WIM-PP-2 cysts of a snow alga (*Trochiscia rubra*) were highly abundant, with some cysts preserved in the stage of cell division (Table **ESM** Table 3; Fig. 10).

5.4. Site 1: Numerical ages

At site 1, two samples for quartz OSL dating and six charcoal samples for radiocarbon dating were extracted from the loess layer. The quartz OSL signals of samples WIM 1 and WIM 11 are fast component dominated (ESM Luminescence dating) and therefore well-suited for age determination using the SAR protocol. The De distributions for both samples show very low overdispersion values and individual De estimates reveal good precisions (<8% relative error), supporting the sedimentological interpretation that these sediment samples are aeolian in origin and were probably well bleached prior to deposition. OSL ages

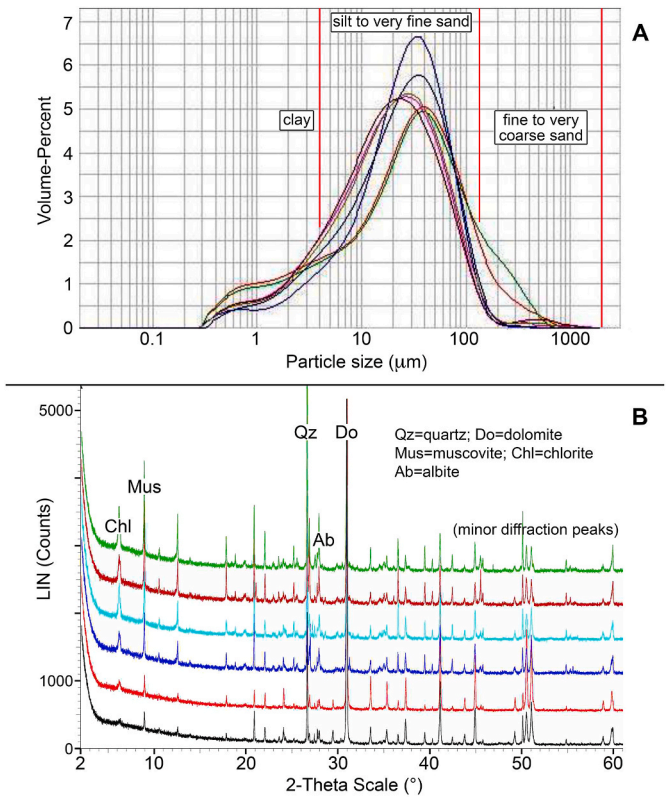

Fig. 6. Site 1. A) Grain size distribution of six samples from the loess layer of site 1. B) X-ray powder diffraction analyses of the mineralogical composition of the loess layer, with main diffraction peaks (labelled) showing mineralogical composition of the loess layer.

of 11.5 ± 1.1 ka and 12.3 ± 1.1 ka were obtained (Table 1). The charred *Pinus cembra* that projected into interval C was radiocarbon dated to ~13.6 cal ka BP, whereas another charcoal fragment that was most probably reworked yielded a radiocarbon age of ~13.1–13.2 cal ka BP (sample A and D, respectively; Table 2). The ages of four other charcoal samples plot into a time slot of approximately 12.0–11.3 cal ka BP (samples B, C, E and F; Table 2).

5.5. Site 2 Ullafelsen: Sedimentary succession

At site 2 (Fig. 4) the bedrock is overlain by a sedimentary veneer that varies in thickness between 0.1 and 0.3 m. Excavation pits in the wider site 2 area (an archaeological excavation and several soil sections; Fig. 4B) revealed that this sediment veneer can be subdivided from bottom to top into three sedimentary units (Fig. 11 and 12A; **ESM** Fig. 7; Geitner et al., 2011, 2014): Unit 1 is composed of very poorly-sorted angular pebbles to small cobbles of bedrock a and a matrix consisting of clay to coarse sand(**ESM** Fig. 8A). Thin section petrography of unit 1 reveals (i) a high porousity of the matrix that is rich in large mica flakes and in soil peds, (ii) quartz clasts with microcracks and (iii) a prevalence of soil crumbs with large mica flakes in the topmost millimetres of unit 1 (Figs. 11 and 12B; **SEM** Fig. 9).

Unit 1 is sharply draped by unit 2, which is a layer a few centimetres in thickness displaying a light grey colour in the field (Fig. 12A). This layer was termed 'light layer' by Geitner et al. (2011) (Fig. 12A) and, as mentioned in the site description above, was used as a seasonal living floor by Mesolithic hunter-gatherers (Schäfer et al., 2016). Unit 2 is characterized by (i) a dominance of the silt to fine-sand grain size fraction (≥90 wt%; **ESM** Fig. 8A; Geitner et al., 2014); (ii) a bulk mineralogy of the lithic sediment fraction composed of plagioclase, quartz as well as micas and chlorite with accessory minerals typical for the metamorphic host rock (**ESM** Table 4; Geitner et al., 2011); and (iii) a compact and organic poor matrix. Unit 3 comprises the top layer and is rich in humus containing many small fragments of charred wood of conifers and woody angiosperms, soil crumbs and granules (Fig. 11; **ESM** Figs. 7 and 10). In the field the boundary to this unit is delimited by

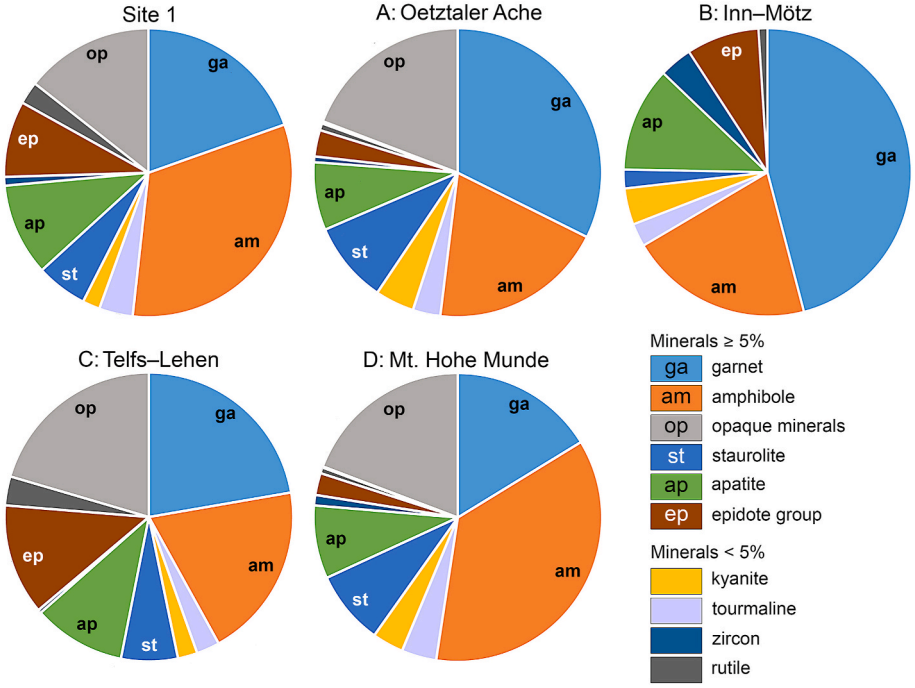

Fig. 7. Comparison of heavy mineral spectra of the loess layer at site 1 with (i) deglacial to early paraglacial loess described in Gild et al. (2018) from the wider site 1 area (samples C and D) and (ii) with heavy mineral spectra of modern fluvial sediments from the rivers Oetztaler Ache and Inn (samples A and B). See Fig. 1B for sample locations.

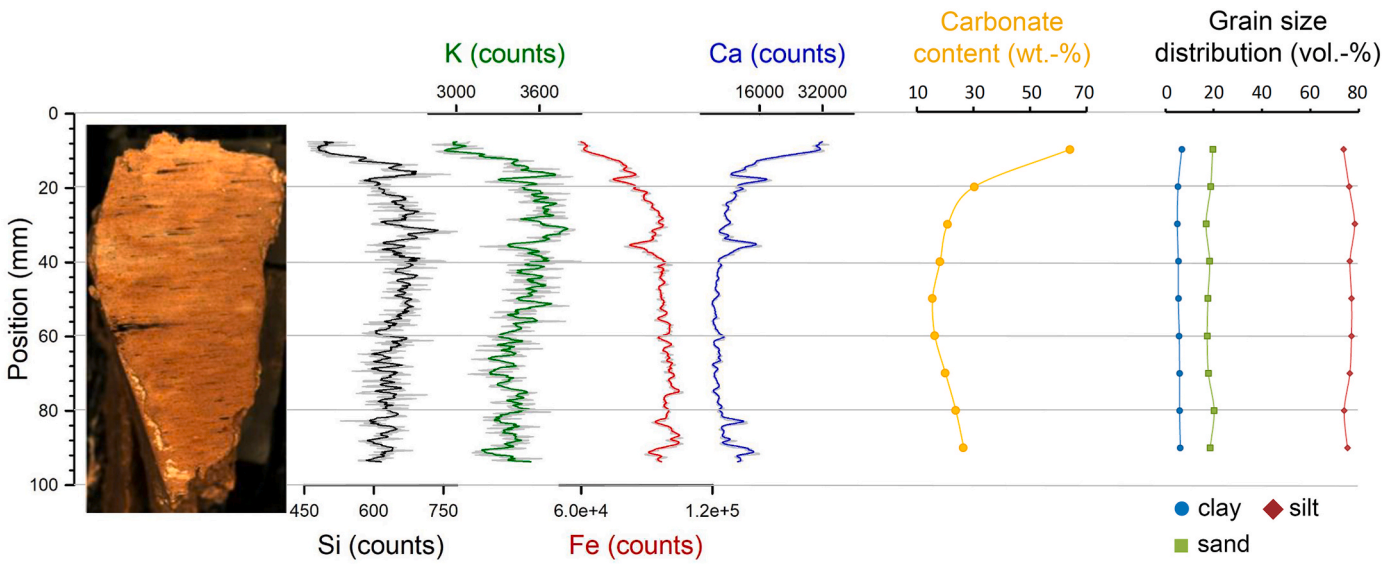

Fig. 8. High-resolution XRF scan of a sediment core of the loess layer at site 1. The core covers the entire thickness of the loess layer at this site.

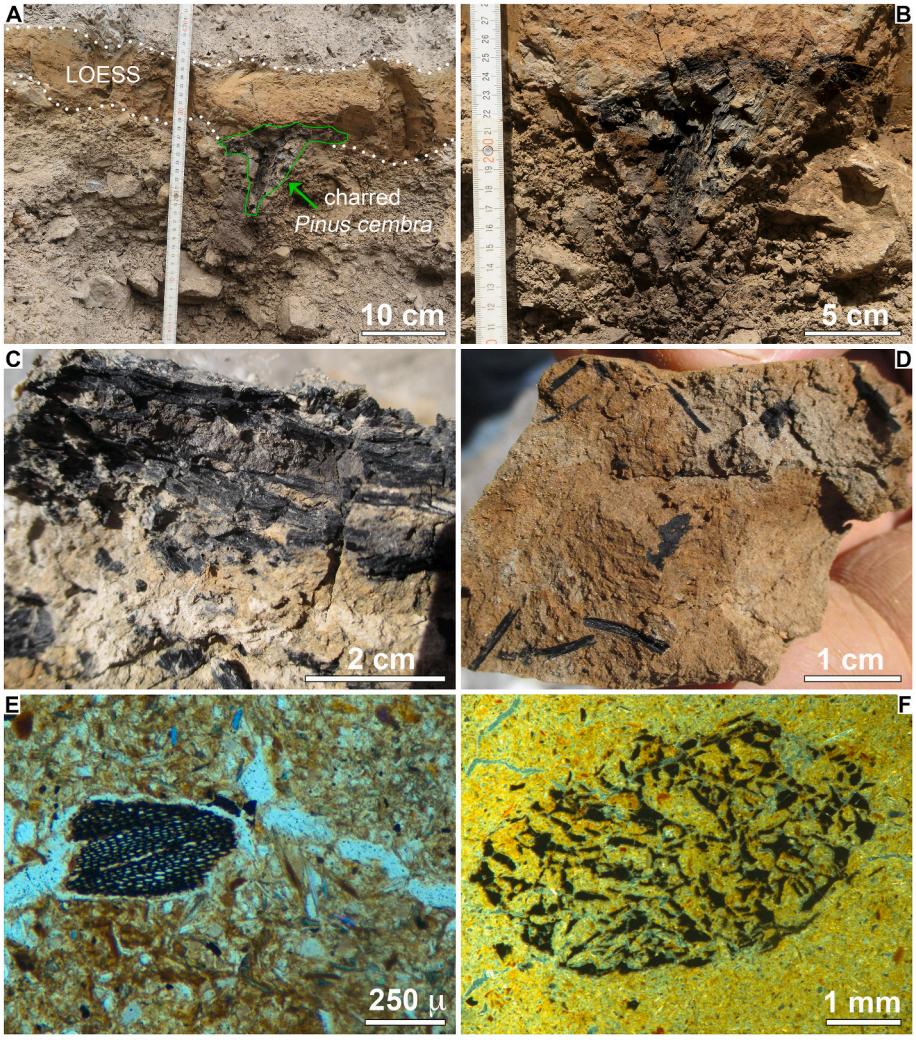

Fig. 9. Macro- and microscopic organic content of the loess layer at site 1. A) Large piece of charred *Pinus cembra* stuck within the topmost part of interval C and projecting into the overlying loess layer. B) Closeup of A showing charred *Pinus cembra* fragment. Larger piece of charcoal (C) and charred conifer needles (D). Thin section images of a charred conifer wood fragment (E; parallel nicols) and a charred Pinaceae microsporophyll likely from *Pinus sylvestris* (F; dark-field illumination).

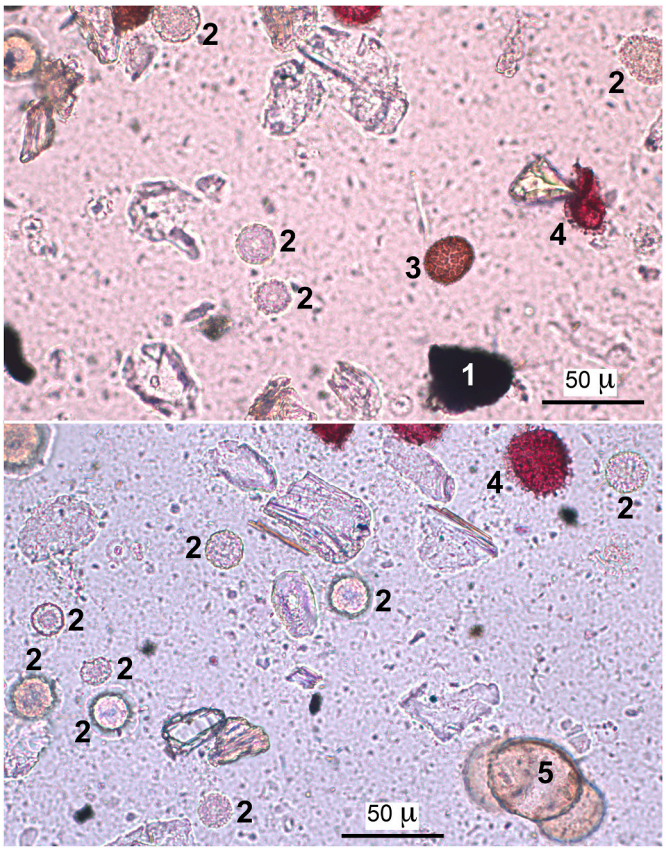

Fig. 10. Microscopic slide of palynological sample WIM-PP-2 from site 1. Aside of minerogenic fragments (not labelled), the sample contains abundant microcharcoal particles (1), abundant chlamydomonadacean green algae, likely *Trochiscia*-cyst stages of a *Sanguina* species (2), a foveolate moss spore of *Enthosthodon hungaricus* (3), spores of *Lycopodium clavatum* added as marker spikes for concentration calculations (4), and well-preserved *Pinus* (pine) pollen (5).

a distinct change in colour (Fig. 12A). In thin sections, however, this transition is less sharp and is mottled by rooting (**ESM** Fig. 10A). Comparison of unit 2 and 3 suggests that they differ in terms of their organic content (unit 2–5 %, unit 3–15 % loss on ignition; Geitner et al., 2011), while the grain size distributions and mineralogical compositions of both units are broadly similar to each other (**ESM** Fig. 8A; **ESM** Table 4).

5.6. Site 2: Numerical ages

The luminescence properties of quartz from site 2 were not suitable for OSL dating, hence, infrared-stimulated luminescence dating (IRSL) dating of feldspar was used instead to constrain the depositional age of unit 2 at this site. The results are discussed in detail in the ESM section on luminescence dating, and are reported here in brief. For IRSL De calculation the central age model and the finite mixture model has been fitted to the feldspar single-grain De distribution and an overdispersion value of 30% (i.e., identical to the overdispersion value obtained from the dose recovery experiment) has been added prior to running the finite mixture model. The statistically most robust solution (David et al., 2007) was obtained via a 3-component fit. The main De component yields an age of 11.6 ± 2.1 ka and is statistically identical with the single-grain feldspar age based on the central age model (10.9 ± 1.8 ka; comprising >50% of the accepted grains. Hence, given the relatively large uncertainty on this IRSL age (16.5% relative error) the period of deposition for unit 2 can be constrained to no better than 12.7 to 9.1 ka, if based on luminescence dating alone (Table 1).

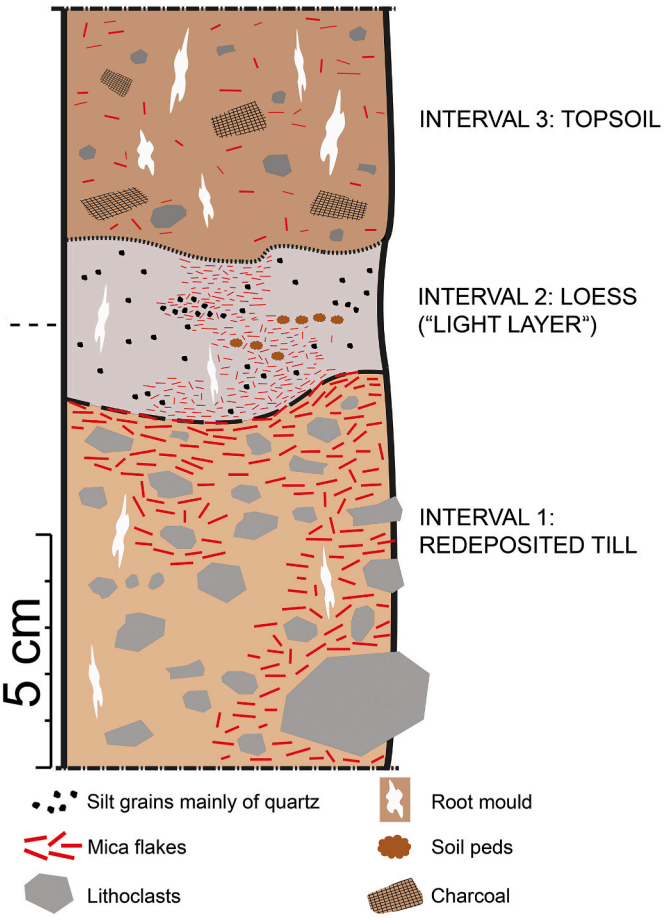

Fig. 11. Schematic sediment log of site 2 (Ullafelsen). See text for further description.

From the Mesolithic living floor of site 2 atop of unit 2, Schäfer (2011) reports 22 radiocarbon ages. We recalibrated these ages using the latest calibration curve (Intcal 20; Reimer et al., 2020, Table 2). The calibrated ages range from 10.94 ± 0.41 cal ka BP to 9.5 ± 0.10 cal ka BP with a weighted mean age of 10.44 ± 0.12 cal ka BP.

6. Discussion

6.1. The loess layer at site 1

The lateral extent of unit D (the loess layer) over at least a few hundreds of meters, and its overall constant thickness, grain-size distribution of fine to coarse silt, and polymictic mineralogical composition support an interpretation of this sediment as loess (Muhs, 2013; Vandenberghe et al., 2018, Fig. 6). XRF and microscopic investigations do not indicate a distinct internal layering or changes in sedimentation, supportive of constant aeolian depositional conditions (Fig. 8). Thin section observations also suggest limited bioturbation (mottling) in the top part of the layer, whereas the isolated sand-sized dolostone fragments that float in the topmost part of the loess layer may have arrived by aeolian transport too (e.g. via traction or saltation during strong wind gusts; Fig. 5). The lenses of angular, fine-to medium dolostone pebbles locally embedded into the layer (Fig. 5C) indicate events of limited surface runoff that was not sufficient to erode the aeolian deposit.

Geomorphological and sedimentological observations further suggest that the loess layer was probably deposited onto a dormant palaeofan surface, because the loess layer drapes the underlying units B and C with a large fragment of a stone pine stuck with its lower part in interval C and projecting into the loess layer (Figs. 5 and 9). Lateral migration of

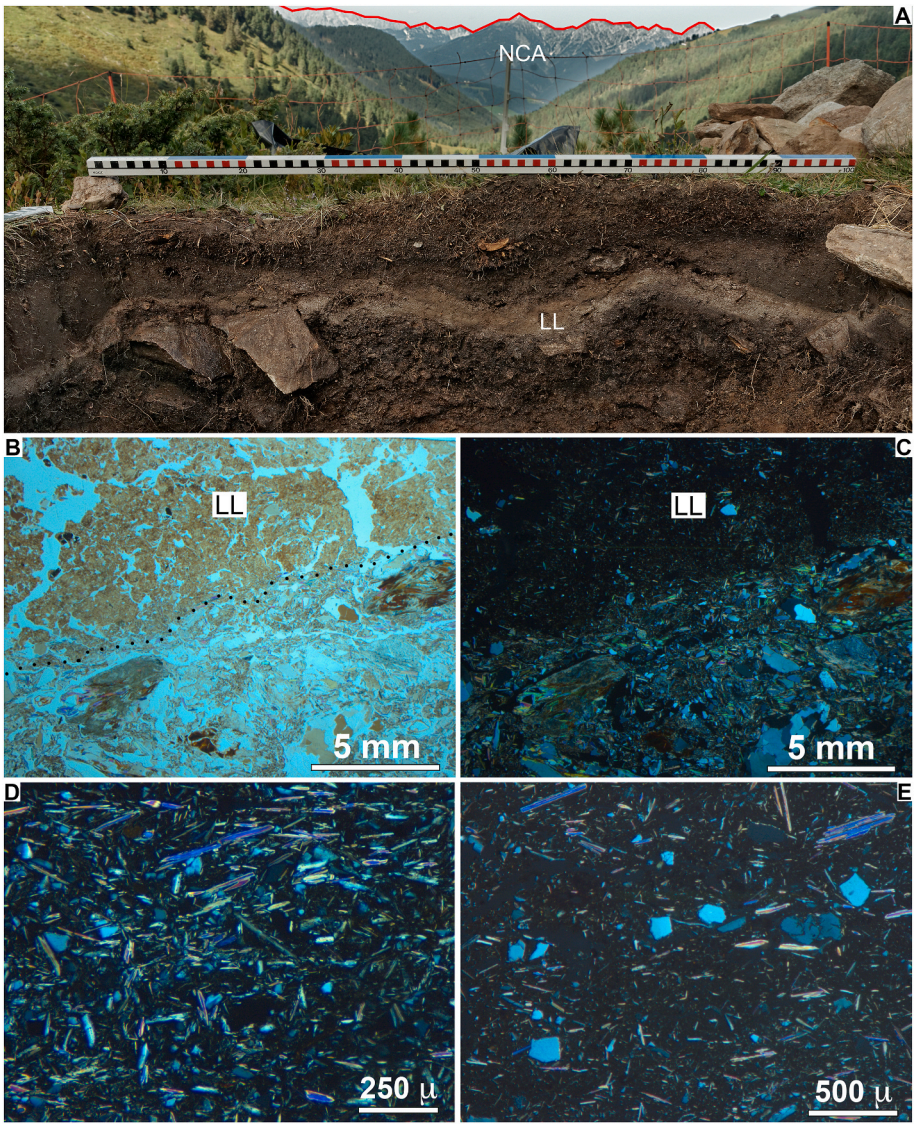

Fig. 12. Sedimentary succession and petrographic thin section observations at site 2. A) Northernmost excavation quadrant (C9N; compare Fig. 4B) showing sedimentary unit 2 (loess layer, LL) draping over unit 1. The luminescence sample for IRSL dating has been obtained from the loess layer in this outcrop face. In the background the Northern Calcareous Alps (NCA) and the Inn Valley are visible. B and C: Petrographic thin section images showing sharp transition between unit 1 and the loess layer (LL; unit 2) under parallel (B) and crossed (C) nicols. The loess layer consists of subangular blocky peds of variable size and displays quartz grains and mica flakes in a much smaller grain size (fine-sand to silt) compared to the over- and underlying units. D and C: Petrographic thin section close-ups showing crumble ped of the loess layer with abundant small mica flakes embedded in soil with a few vuggy pores (D, crossed nicols) and organic-rich soil ped with a few angular grains of quartz and abundant small mica flakes (E, crossed nicols).

the feeder channel as the cause for a temporary shutdown of alluvial fan aggradation that allowed for aeolian accumulation is excluded, because (i) the alluvial-fan succession at site 1 is laterally confined by adjacent fans, indicating that the feeder channel had little freedom to switch laterally (Fig. 3), and (ii) the exposed minimum upslope extent of the loess layer and its dip (representing the dip of the fan palaeo-surface ~11 ka ago) that is similar to the dip of the present alluvial fan surface support the interpretation that the fan surface was abandoned of alluvial deposition before loess accumulation, and that the contact between units B + C with D represents a hiatus of an unknown time span.

With respect to mineralogical composition, grain size distribution and heavy mineral spectrum the loess layer of site 1 is indistinguishable from the older Late Glacial loess that occurs in the vicinity of site 1 at higher altitude (samples C and D in Figs. 1 and 7), and is also indistinguishable from the fine-grained fluvial sediments of the adjacent Inn River and its tributaries (samples A and B in Figs. 1 and 7; Gild et al., 2018). On sedimentary petrographic grounds it is thus concluded that loess at site 1 must have been sourced locally from areas where polymictic deposits were exposed to deflation. Likely scenarios include (i) deflation from the nearby Inn Valley floor during times when aggradation and braided river conditions were prevailing, (ii) deflation from glacial outwash plains of mountain glaciers in the crystalline catchments ~10 km south of the Inn River, and/or (iii) deflation from areas covered by Late Glacial loess when subjected to vegetation thinning and wildfires. Scenario (i) is deemed particularly plausible, because silt is effectively produced in glacial land systems, especially along braided streams where continuous reworking of sediment and exposure to deflation is highly effective (Bullard and Austin, 2011; Muhs et al., 2013; Zhang et al., 2015; Wolfe and Lian, 2021).

The palynological evidence from the loess layer at site 1 suggests the following: The presence of *Entosthodon hungaricus* indicates cold and/or dry environmental conditions during loess formation, as this moss characterizes steppic vegetation on carbonate-rocky terrains, and today is typical for dry areas in eastern and southern Europe and the Levant

(Boros et al., 1993; Cano et al., 1999; Ahrens, 2000).

The charred stone pine stuck in interval D and projecting into the loess layer and the relatively abundant charcoal fragments floating within the loess suggest that aeolian deposition might have been accompanied by wildfires, promoting potential reworking of the older Late Glacial loess layer (Wagenbrenner et al., 2013; Schaetzl et al., 2021).

The pollen sample taken from the base of the loess layer contains chlamydomonadacean snow-algal cysts at high concentrations (>27000 cysts per cm^3), with a few cysts preserved in the stage of cell division. Snow algae bloom and produce cysts in melting snow, typically from spring to summer and today thrive in the Alps at altitudes >2000 m asl. (Kol, 1968; Hoham and Remias, 2020). This suggests that, at least at the sampling position, the lower part of the loess layer accumulated in spring, perhaps over a short time period. All other pollen types occur at very low concentrations only (ESM Table 3) in line with an interpretation of overall rapid dust accumulation.

Next, we evaluate whether an absolute loess accumulation rate can be inferred from the data of site 1. The difference between the radiocarbon age of the stone pine stuck in interval C and projecting into the loess layer (~13.6 cal ka BP), and the charcoal pieces near the top of the loess layer (maximum age range from 11.7 to 11.2 cal ka BP, Table 2) might be interpreted as an indication for persistent loess deposition over approximately 1.9–2.4 ka with a mean accumulation rate of ~ 0.8–0.9 mm/year. This, however, contrasts with the evidence provided by pollen and snow-algal cysts suggestive of much more rapid loess accumulation at site 1.

Comparison with documented rates of dust accumulation suggest that high accumulation rates can be attained e.g. under full glacial conditions (typically ≤ 1 mm/year; Eagar et al., 2017; Kohfeld and Harrison, 2001; Frechen et al., 2003), while under highly favourable pro- and fluvio-glacial conditions accumulation rates can ramp up to >10 mm/year, as in the case of Late Glacial loess deposits in Nebraska (Roberts et al., 2003) or in the Canadian Rockies, where an ephemerally-submerged braidplain ~1.5 km in width provides wind-blown silt to the adjacent landscape (Hugenholtz and Wolfe, 2010). It is noted that 10–30% coverage of the land surface by grass can substantially increase the accumulation rate of aeolian sediment relative to barren ground by 100% and more via filtering aeolian material from the sediment-laden airflow (Yan et al., 2011). We conclude that loess accumulation rates at site 1 cannot be pinpointed precisely, but are broadly in-line with documented glacial to late glacial rates and might have been temporarily very high (>10 mm/year for the lower part of the loess layer), maybe as a result of extreme dust storms in combination with filtering of aeolian sediment by a thin vegetation cover.

6.2. The sedimentary succession at site 1

Clast lithologies combined with the extremely-poor sorting and faint bedding, indicates that unit A accumulated mainly from cohesive debris flows supplied by redeposition of till plus scree from local rocky slopes (**EMS** Fig. 5**, EMS** Table 2). The slope facets between the alluvial fans (Fig. 3B) consist of *in-situ* and redeposited LGM till. Hence, unit A probably accumulated during the waning paraglacial phase, i.e. when till and clastic material was redeposited from the adjacent mountain flank immediately subsequent to the LGM. Depositional unit B composed of angular dolostone scree accumulated from sheet flows, perhaps due to upslope exhaustion of erodible till. Alternatively, or in addition, stabilization of the source area by vegetation may have led to prevalent sheet flow deposition. Unit C accumulated from cohesive debris flows and overlies unit B conformably or disconformably, depending on outcrop position. Units B and C are draped by the loess layer (unit D) that has been OSL dated to ~11–12 ka (Table 1A). This facies shift suggests a distinct change in the sedimentary environment around that time towards high dust loading of the atmosphere. In unit E the faint stratification of the poorly-sorted dolostone scree with a matrix of carbonate mud suggest debris flow deposition, while the slight yellowish tint of the matrix of unit E indicates partial reworking of the underlying loess layer and/or continued input of airborne siliciclastic dust while fan deposition had resumed (**ESM** Table 2**; ESM** Fig. 6E). Unit E might comprise the Early to Middle Holocene section of the Wildermieming fan succession, while the topmost unit F (sheet flow deposits) probably aggraded until recently, based on aerial photographs from 1974.

Mixed alluvial fan/aeolian deposystems, as encountered at site 1, are typical for cold or hot, relatively dry areas (Langford, 1989; Latrubesse et al., 2012; Wolfe and Lian, 2021), including the hyper arid Atacama Desert (Ventra et al., 2013). For a paleoclimatic interpretation of the site 1 sediment succession the following observations are critical: Firstly, for the dynamics of such mixed deposystems, climatic aridity and/or pronounced wet/dry seasonality is more decisive rather than mean annual air temperature (Langford, 1989; Wolfe and Lian, 2021). Secondly, the preservation of a loess drape in an alluvial-fan setting requires a transient halt or marked lowering of surface runoff, suggestive of a switch to a drier climate, because such a fine-grained loose sediment drape would otherwise be easily eroded. Both observations fit with rapid cooling, aridification and enhanced storminess and seasonality during the Younger Dryas (Denton et al., 2005; Brauer et al., 2008), In contrast, sparsening of the vegetation cover due to climatic cooling and/or by wildfires, but at constant rates of precipitation should lead to an increase of slope-derived sediment input and fan aggradation and erosion of any synchronously forming fine-grained and loose sediment drapes (Sass et al., 2006,2010; Schneider et al., 2010; Larsen et al., 2013).

6.3. The loess layer at the Mesolithic Ullafelsen (site 2)

Site 2 was last covered by a local valley glacier during the early part of the Late Glacial, i.e. most probably during the Gschnitz stadial ca. 15.4 ka ago, while the site was ice-free during and subsequent to the YD (Ivy Ochs et al., 2005, 2008, Kerschner, 2011, Fig. 4). Hence, the pebbly to cobbly angular material of unit 1 is interpreted to originate in large parts from glacial drift and lateral moraines mobilized during the meltdown of the Gschnitz valley glacier. This is in line with the observation that the lithoclasts in unit 1 are rich in microcracks, which we interpret as the result of subglacial loading (**ESM** Fig. 9B). The grain-size distribution of unit 2 (fine silt to fine sand; **ESM** Fig. 8) suggests an aeolian origin of this unit. This interpretation is supported by the geomorphological position of site 2 positioned on a bedrock ledge ~60 m in altitude above the valley thalweg, and ~6 m above and 30 m laterally off the toe of the adjacent scree slope. In this isolated and elevated position of site 2 practically no other process except of aeolian fallout can explain the presence of such a fine-grained sedimentary drape, because (i) a mass flow would have to spill uphill over 6 m in altitude to reach the site (Fig. 4B), and (ii) would thus no longer be a gentle shallow flow selectively carrying fine-grained material only, but rather a massive debris flow transporting much coarser-grained clasts. The few sand-to fine pebble-sized rock fragments present at the top of the unit 2 are thus best explained by snow avalanche transport. Furthermore, the soil matrix observed in unit 2 suggests the presence of a vegetation covered with grass or small shrubs that favoured trapping of aeolian material.

In the topmost unit 3, the common fragments of charred wood, the humus-rich soil matrix and the presence of only few mineral fragments of silt-to coarse sand size suggest that this unit is the result of soil formation since the Early Holocene.

Unit 1 and 2 were subject to weathering and overprinting by these soil-formation processes, mainly via podsolization (Zech et al., 2021). We dismiss the possibility that the formation of unit 2 resulted solely from podsolization of the underlying unit 1, because of the numerous pebble-sized fragments in unit 1 that were to be expected in unit 2 under a podsolization scenario, but are absent. Finally, phyllosilicates in unit 2 are consistently much finer-grained than in the underlying unit 1, again

supporting an aeolian origin of unit 2 (Fig. ESM Fig. 8).

6.4. Timing of loess deposition at site 1 and 2

The luminescence ages (**red dots in** Fig. 2) of the loessic sediments from both sites comprise a time range of ca. 1.4 ka extending from 12.3 to 10.9 ka (weighted mean age 11.8 ± 0.7 ka; Tables 1A and 1B). The error ranges of the luminescence ages might in principle allow to assign loess deposition at both sites to the YD. Yet, they are also congruent with the Preboral oscillation (PBO ~11.3 cal, ka BP; Fisher et al., 2002; Bos et al., 2007) (Fig. 2) during the earliest Holocene.

Six charcoal samples were obtained from site 1 (Table 2) and their calibrated radiocarbon ages are also plotted in Fig. 2. Two of these six charcoal pieces are of Bølling-Allerød age, i.e., samples A and D, and the former is still stuck in unit C and projects into the overlying loess layer. Sample A is interpreted as a charred, but in situ root, and the calibrated ^{14}C age of 13.64 ± 0.12 ka cal BP of this sample thus provides a maximum age for the loess layer of site 1. It is frequently observed that old charcoal can be preserved within, e.g., alpine soils or sediments and can get incorporated into younger sedimentary units during periods of landscape instability due to erosion and redeposition (Carcaillet, 2001; DeLong and Arnold, 2007). Hence, the second charcoal sample that is of Bølling-Allerød age and thus predates the YD time interval (sample D; ~13.1 cal ka BP), but is contained in the loess layer of site 1, is interpreted as such a re-deposited organic material. Sample D hence provides a maximum age for the loess layer at site 1, too. Three charcoal ages overlap or just overlap with the YD time interval (samples B, C and E), and only one charcoal age (sample F) plots clearly outside the YD (Fig. 2, Table 2). Conversely, samples B, E and F are – within error – also congruent with the cold phase of the PBO (Fig. 2).

At site 2 twenty-two charcoal fragments were collected from the top of unit 2, which served as a living horizon for Mesolithic hunter-gatherers, and have been radiocarbon dated by Schäfer (2011b) (Table 2). After removal of one obvious outlier (sample u), the calibrated 14C ages span a time range from 10.9 ± 0.2 to 9.5 ± 0.05 cal ka BP (Table 2). The oldest charcoal samples date to 10.9 ± 0.2 cal ka BP are (weighted mean of the six oldest ages, making up 30% of the entire dataset) and are the earliest indication for human presence at site 2. The radiocarbon datum of 10.9 ± 0.2 cal ka BP is thus interpreted as a firm minimum age for the underlying loess layer. The IRSL single-grain age of 11.6 ± 2.1 ka determines the depositional time of the loess itself and because of the overlying radiocarbon age control, loess accumulation can be constrained to a time window from 13.8 ka to 10.9 ka BP, based on IRSL and the oldest calibrated radiocarbon ages and their respective uncertainties. Furthermore, site 2 was covered by ice during the advance of the local valley glacier during the Gschnitz stadial at ~15.7 ka (Ivy Ochs et al., 2005, 2008; Kerschner, 2011), putting an upper age bound on loess deposition at Ullafelsen. Thus, also at site 2, aeolian deposition could be attributed to the YD as well as to the PBO (Fig. 2).

Taken together, these observations require further discussion, because at first sight no unequivocal attribution of loess accumulation, neither, at site 1, nor at site 2 to the cold and arid dry spell of the YD appears to be possible. Yet, at both sites the YD might be regarded as the most probable climatic trigger event for intensified aeolian activity. In the following, different types of environmental records from the YD to the earliest Holocene are briefly summarized, with an emphasis on the Eastern Alps: (1) speleothems, (2) glaciers and rock glaciers, (3) lakes and peat bogs as well as (4) fluvial systems. An attempt is made to put the inner alpine loess record from Wildermieming (site 1) and the Fotsch Valley (site 2) onto a common timeline to facilitate regional proxy comparison and a proper palaeoenvironmental interpretation.

6.5. The Pleistocene-Holocene transition chronicled in alpine sedimentary archives

Speleothems from different locations in the Eastern Alps consistently record the YD as a significant negative δ^{18}O excursion of spelean carbonate lasting from ~13.0–11.8 ka (Wurth et al., 2004; Li et al., 2021). Quantitative temperature estimates based on spelean δ^{18}O suggest that the transition from the Bølling-Allerød into the YD was associated with a drop of ≤3 °C in mean annual air temperature (MAAT) and relatively snow-rich winters in the early part of the YD, while the YD/Holocene transition was associated with a warming of 4–5 °C (Koltai et al., 2021; Li et al., 2021). Further cold oscillations, albeit at low to very low intensity in terms of their δ^{18}O amplitude, are recorded in alpine speleothems, including the PBO at ~11.3 ka and further cooling events at ~10.2 ka, ~9.1 and ~8.2 ka (Boch et al., 2009; Li et al., 2021). In general, high resolution speleothem records from the Eastern Alps suggest that the earliest Holocene was climatically more unstable compared to the Middle and Late Holocene. Yet, because spelean δ^{18}O is primarily depicting atmospheric processes, no direct insights into earth surface processes are gained by these archives (Henderson, 2006; Meyer et al., 2012; Töchterle et al., 2023).

Valley glaciers are generally deemed accurate (paleo)climate indicators that react sensitive to temperature changes (Oerlemans, 2005). Alpine valley glaciers re-advanced subsequent to the warming of the Bølling-Allerød, depositing the so-called Egesen moraines, i.e. a latero-frontal moraine system often composed of two or more closely nested but individual ridges. (Kerschner and Ivy-Ochs, 2008; Ivy-Ochs et al., 2009; Moran et al., 2016a; Baroni et al., 2017). Terminal moraines located several kilometres up-valley from the Egesen moraine system, yet outside of the Little Ice Age moraine stage, have been identified as well in the Alps and were termed Kartell stage (Fraedrich, 1975). Numerical dating of these moraines supports a broad correlation of the Egesen maximum advance with the early YD, and of the Kartell stage with the PBO (Fig. 2) (Kerschner and Ivy-Ochs, 2008; Ivy-Ochs et al., 2006, 2009). Furthermore, enhanced rock glacier activity is broadly concomitant with these glacial advances in the Eastern Alps (Moran et al., 2016b; Ivy-Ochs et al., 2009; Steinemann et al., 2020).

Records of peri-alpine lakes of the Eastern Alps indicate significantly increased input of fine-grained lithic material during the YD (Lauterbach et al., 2011; Daxer et al., 2018). This may be related to (i) a generally increased storminess during the YD (Brauer et al., 2008), (ii) treeline lowering by 400–500 m in altitude relative to the present (see, Bortenschlager, 1992; Rey et al., 2013; Heiri et al., 2014) and/or (iii) a change in low-to mid-altitude forests from closed thermophilous forests during the Bølling-Allerød to open forests and steppe-like grasslands during the YD (Tobolski and Ammann, 2000; Ammann et al., 2000; Vescovi et al., 2007; Lauterbach et al., 2011).

Four peat bogs located between 34 and 75 km east of site 1 provide insights into the climate and vegetation dynamics during the Pleistocene Holocene transition in the Inn Valley itself. The pollen record from the first peat bog (Lake Lans; 840 m asl.) indicates that ice-free steppe-like conditions prevailed since ~17.5-16 ka BP in the Inn Valley and reforestation with pine and birch started shortly after 16 ka BP (Bortenschlager, 1984a). During the YD open forest of pine and birch persisted. At ~11.7 ka BP, a mixed oak forest established and thrived at least until 10.75 ka BP (end of pollen record; Bortenschlager, 1984a). A similar vegetation history is recorded by the other three peat bogs (Zotensenk, Krumsee and Lindenmoor; Bortenschlager, 1984b): During the Bølling-Allerød rapid reforestation by betula and pinus occurred. The YD is recognized as a rise of non-tree pollen and cold-loving vegetation as well as juniperus and hippophae. Pinus distinctly decreased during the YD, while betula persisted, indicating an opening of forests. The regional treeline probably lowered from ~1800 m asl to ~1500 m asl during the YD. Subsequently, the appearance and rise of warm-loving deciduous trees and bush, such as Ulmus, Tilia, Quercus and Corylus represent the onset of the post-YD warming (Bortenschlager, 1984b).

Geoarchaeological data from mid-to high altitude settings in the Trentino region (southern Alps ~130 km south of the Inn Valley) suggest that the YD was a phase of rejuvenated loess deposition in a steppe-like environment, while on bottoms of trunk valleys, coarse-grained braided

streams reappeared during that time (Castiglioni et al., 1990; Angelucci and Bassetti, 2009).

The fluvial record of the Inn River is constrained via a series of sites from the inner-alpine stretch of the river as well as from the alpine foreland. A fluvial terrace succession deposited by the Inn ~125 km downstream of site 1 and 2 in the alpine foreland reveals a total of 7 terrace levels. These terraces were investigated and partly numerically dated by Megies (2006). According to Megies (2006) the oldest and highest-positioned terrace formed during the LGM, followed by a series of lower, presumably Late Glacial terraces. One of these lower discrete terrace levels has been radiocarbon dated to the beginning of the YD (13.4 ± 1.1 ka, 12.7 ± 1.1 ka; notation by Megies, 2006). Some of the lower terrace levels were ascribed to fluvial aggradation during the PBO and the 8.2-ka cooling event by Megies (2006), but yet lack numerical age control. The Late Glacial terraces are covered by loess that has been IRSL dated to 16–14 ka (Terhorst et al., 2002).

Our current understanding of the inner-alpine fluvial dynamics of the Inn is based on a series of sites located mainly within the city of Innsbruck as well as several km eastward of the city. Prior to the LGM the Inn Valley floor aggraded rapidly as evidenced by outcrops in erosional terraces located at ~200–250 m above the modern Inn level, revealing pebbly proglacial outwash that interfingers with and is overlain by basal till of the LGM (Patzelt and Resch, 1986). The onset of this proglacial outwash deposition has been dated to 33-32 cal ka BP BP at the location Baumkirchen (Spötl et al., 2014) situated ~44 km downstream of site 1 Wildermieming. The fluvial dynamics and valley floor evolution subsequent to the LGM is constrained by radiocarbon dated wood pieces (16.9–15.4 cal ka BP) and reindeer bone (14.9–14.15 cal ka BP) buried 21.6 m and 16 m below the present floor of the Inn Valley, respectively (Patzelt, 2014), as well as by a tree fragment recovered from pebbly stream deposits at the location Innsbruck-hospital (15.2 ± 0.28 cal ka BP; Patzelt and Weber, 2015) (Table 2). Approximately 18 km east of Innsbruck, organic remnants within fine-grained overbank deposits located 3.5 m below the present valley bottom were dated to 11.2 ± 0.48 cal ka BP (Patzelt, 1987, 2014) (Table 2). These observations and numerical data from the Inn Valley suggest (i) rapid and pronounced valley floor aggradation in the forefront of an advancing ice-stream network immediately prior to the LGM followed by (ii) pronounced valley floor incision during the LGM via glacial erosion and/or via fluvial incision subsequent to LGM, and (iii) fluvial aggradation pulses during the Late Glacial and probably during the YD too. No conclusive data for the valley floor development during the earliest Holocene (e.g. the PBO) exist so far from the inneralpine-stretches of the Inn River. The middle and late Holocene was characterized by re-incision and an alternation of minor river aggradation and re-incision, but the Inn Valley floor level of the Latest Pleistocene was not attained again (Patzelt and Weber, 2015).

In the Southern Alps the Bølling-Allerød valley floor of the Adige Valley (provinces of Southern Tirol and Trentino) is located more than 130 m below the modern valley level. Drill cores as well as geophysical and radiometric data indicate that alluvial deposits of the YD significantly contribute to this fluvial aggradation (Fuganti et al., 1998). Similar results are obtained for other major valleys of the Southern Alps, such as the Brenta Valley, a major tributary to the Adige valley (Felber et al., 2000).

We summarize the evidence that comes from speleothems, glaciers and rock glaciers, pollen records as well as fluvial archives at the Pleistocene-Holocene transition in the broader investigation area as follows: (i) in spelean $\delta^{18}O$ the YD is chronicled as a severe cold event (~3 °C MAAT cooling compared to the Bølling-Allerød), but the PBO and a series of smaller cooling events at the beginning of the Holocene are recorded in some alpine speleothems too (Li et al., 2021; Koltai et al., 2021); (ii) glacier re-advances and enhanced rock glacier activity are well documented for the YD (Egesen moraines) and the PBO (Kartell moraines; Moran et al., 2016b; Ivy-Ochs et al., 2009; Steinemann et al., 2020); (iii) peri- and inner-alpine pollen records, including records from the middle Inn Valley, indicate a change from closed thermophilous forests that prevailed during the Bølling-Allerød to open forests and steppe-like grasslands at the beginning of the YD and a concomitant increase of atmospheric dust loading (Bortenschlager 1984a, 1984b; Brauer et al., 2008; Angelucci and Bassetti, 2009; Lauterbach et al., 2011). The PBO and early Holocene cold events are not well resolved or recorded in these organic archives; (iv) fluvial archives reacted sensitively to severe cold events causing pronounced valley floor aggradation, e.g. prior to the LGM as well as during Late Glacial cooling events, including the YD. This holds true for inner-alpine valley stretches of the Inn as well as for the Inn River in the alpine foreland as well as the southern Alps (Fuganti et al., 1998; Patzelt, 2014; Megies, 2006; Spötl et al., 2014). The inner-alpine fluvial record for the PBO and other early Holocene cooling events is – given the current data availability – not conclusive.

6.6. *Timing and climatic control of dust flux, fluvial aggradation and braiding in the Inn Valley*

The causal links between climate, fluvial aggradation and aeolian sediment dynamics are relatively well established. Climatic cooling, if significant enough in relation to a given catchment and its internal threshold parameters, will lead to an increase in physical weathering and thus scree production alongside with sparsening of vegetation (Van Husen, 2000; French, 2007; Murton et al., 2006; Hales and Roering, 2009). On a catchment scale the combination of these biotic and abiotic processes causes an increase in fluvial bedload eventually leading to valley floor aggradation. In terms of fluvial morphodynamics and channel patterns climatic cooling typically initiates a transition from meandering or anastomosing rivers to braided rivers or increases the braiding activity in an already braided stream, which is true particularly for intramontane settings (Hallet et al., 1996; Van Husen, 2000; Vandenberghe, 2003; Ashmore, 2022). As such, braid plains are highly effective sources of aeolian silt due to an almost continuous reworking of sediment by rapid lateral shifting of channels and bars and repeated overbank flooding (Nickling, 1983; Good and Bryant, 1985; Smalley et al., 2009; Hugenholtz and Wolfe, 2010).

As outlined, the YD environmental conditions along the lower and middle stretches of the Inn Valley were characterized by a sparse and patchy vegetation, strong seasonal frost and enhanced braiding activity. We therefore suggest that YD braid plains of the Inn River were the primary source of aeolian material for the loess layer at site 1. Furthermore, 15 km upstream of site 1 the Inn River is joined by one of its major tributaries, the Oetztaler Ache (Fig. 1B), and this confluence probably formed an extensive local deflation area during the YD. We further speculate that (i) the cold-dry climatic conditions that prevailed during the YD in the Eastern Alps increased wildfire frequency around that time (Kerschner et al., 2000; Hao et al., 2023), as hinted to by the high concentration of charcoal in the loess layer at site 1, and that (ii) loess that had been deposited and draped over the alpine landscape immediately subsequent to the LGM (Gild et al., 2018) was re-activated by these wildfires, further enhancing dust loading of the air and loess accumulation in these inner-alpine settings.

A similar chain of arguments applies to loess accumulation at site 2. Here the obvious source of aeolian material was the proglacial outwash plain of the local valley glacier. During the YD this outwash plain must have become highly active, because the valley glacier re-advanced and stabilized at a position only 2 km upstream from the site (Fig. 1). Furthermore, local foehn winds likely supported an enhanced dust loading of the air and thus loess accumulation at site 2.

These paleoenvironmental considerations fit with the simplest chronological scenario for site 1 and 2, i.e. loess deposition during the YD. Such a scenario is supported by the quartz OSL ages at site 1 that yielded a weighted mean age of 11.8 ± 0.7 ka and is also broadly consistent with the radiocarbon ages at site 1 (Table 2; Fig. 2). At site 2 the single-grain IRSL age of 11.6 ± 2.1 ka from the loess unit combined

with the weighted mean radiocarbon age of the oldest charcoal pieces from the overlying Mesolithic living floor (10.9 ± 0.2 cal ka; Table 2, Fig. 2), suggest that by ~10.9 cal ka BP the landscape had stabilized, and hunter-gatherers were using a formerly wind-swept valley spot as hunting outlook and camp site.

We thus propose that the YD should be regarded as the climatic trigger that shifted the landscape and environmental processes in these inner-alpine settings of the Eastern Alps towards enhanced supply of aeolian dust and was likely responsible for the bulk of loess accumulation at site 1 and 2. Yet, the numerical ages at both sites are also congruent with loess deposition during the PBO dated to ~11.3 cal ka BP by e.g. Fisher et al. (2002) or Bos et al. (2007). However, compared to the YD the PBO has no or a much weaker geomorphological expression in the alpine landscape and might thus, at least for our investigation sites, be regarded as an ancillary event. So, the possibility that aeolian activity sustained from the YD into the PBO or resumed during the PBO in a subdued manner, is not excluded, particularly at site 2 given its high elevation setting and proximity to a valley glacier and its outwash plain.

6.7. Inner-alpine loess occurrences and their implications

The presence of inner-alpine loess was known to 19th century regional geologists, but the knowledge about these patchy occurrences of silt almost fell forgotten and in the absence of numerical ages it was always assumed that these sediments must result from a single depositional phase subsequent to the LGM (Kravogl, 1873; Blaas, 1885; Küfmann, 2003). The loess layers at site 1 and 2, numerically constrained by luminescence and radiocarbon dating, provide the first record of YD to earliest Holocene loess deposition within the Eastern Alps, and, together with the Late Glacial loess occurrences in the Northern Calcareous Alps OSL dated to ~18 ka (Gild et al., 2018), allow us to refine the concept of inner-Alpine loess accumulation (Fig. 2).

The first and probably most widespread loess deposition took place event-like during and shortly after the down-wasting and decay of the LGM alpine ice-stream network around 18 ka BP (Gild et al., 2018). We suspect that during this first phase a landscape-wide loess layer formed, draping entire mountain flanks up to nunataks, and that loess accumulation was sourced from freshly deglaciated areas, debris-covered dead ice terrain and subordinate from floodplains. We term these deposits that resulted from aeolian processes immediately after the LGM early deglacial loess. The rate of loess deposition probably decreased toward the Bølling-Allerød and was likely minimal during this interstadial but still present as a weak background sedimentary signal The cold-arid climate of the Younger Dryas allowed inner-alpine loess production to kick-in again. We suggest that depending on the topographic setting, more localized veneers of aeolian silt yet still hundreds of meters to perhaps a few kilometres in lateral extent, were deposited during that time, again as an event-like sedimentary process. This pattern of aeolian sediment dynamics might have been sustained until the early Holocene and, depending on altitude and topographic setting, was sourced e.g. by braided stream sections and pro-glacial outwash plains. A rare Holocene example is provided by a localized loess deposit up to 1 m in thickness within a karst doline on a deglaciated plateau at Zugspitzplatt (2290 m asl.; Northern Calcareous Alps), that has been radiocarbon-dated to 8.3 ± 0.16 cal ka BP (Table 2; Grüger and Jerz, 2010). In addition, early deglacial loess might have been partly reworked and mixed with or draped by younger loess.

Even today aeolian sediment is transported and deposited in inner-alpine areas, such as Saharan dust or mineral dust derived by year-round foehn winds from metamorphic rock terrains of the Central Alps (Peer et al., 2022). Yet, the amount and depositional rate of modern aeolian material are much too low to form any macroscopically recognizable layers of loess (Küfmann, 2003, 2008; Grashey-Jansen et al., 2014; Peer et al., 2022). An exception from this are the outwash plains of modern valley glaciers that are still effective sources of windblown sand and silt, and that supply laterally limited drapes and lenses of aeolian deposits (Geilhausen et al., 2012; Lieb and Keller-Pirkelbauer, 2022).

7. Conclusions

For two sites in the Eastern Alps, OSL and IRSL dating and radiocarbon ages provide evidence for intramontane loess deposition during the YD to earliest Holocene. At site 1 (Wildermieming), the loess layer is intercalated into an alluvial-fan succession that is preserved in a low altitude setting adjacent to the Inn River, whereas at site 2 (Ullafelsen, a high alpine Mesolithic site), the loess layer is overlying glacigenic deposits and is covered by topsoil. For loess deposition at site 1, we infer a climatic-fluvial feedback mechanism, with intensified braiding of the Inn River during the YD cold spell as the main cause for aeolian deposition. Wildfires that might have occurred even independently of climatic forcing, probably played a major role in landscape destabilization and reactivation of aeolian deposition. For site 2, we suggest that loess deposition is the result of climatic cooling and aridification that was induced during the YD, but, because of the site's proximity to an active glacial outwash plain, eventually lasted beyond this cold spell for several millennia well into the earliest Holocene.

These are the first unequivocal records of aeolian deposition subsequent to the Bølling-Allerød interstadial within the Eastern Alps, and also the first evidence that significant inner-alpine dust transport and accumulation was not confined to a single, early deglacial phase immediately after the LGM (Gild et al., 2018). While previous studies from high-altitude settings in the Eastern Alps had described minor, localized accumulations of Holocene loess, modern dust concentration is generally insufficient to allow discrete loess layers to form. Considering our new and the existing data of loess accumulation in the Eastern Alps, we suggest a concept of inner-Alpine loess accumulation covering the time from the LGM to the Late Holocene that emphasizes multiple discrete phases of aeolian activity and loess deposition that, with time, were decreasing in intensity and lateral spatial extent (Fig. 2).

Our results underscore the potential of aeolian layers as valuable marker horizons that record specific landscape and environmental responses to climate change during the Late Glacial and early Holocene. We suggest that: (i) more attention should be paid to these types of dust deposits that are often inconspicuous and thus easily overlooked, and (ii) that a concerted analytical effort that involves multiple numerical dating techniques and pollen analysis are required to unlock the full potential of these deposits as palaeoenvironmental inner-Alpine proxy records.

CRediT authorship contribution statement

Charlotte Gild-Haselwarter: Conceptualization, Data curation, Fieldwork, Sample processing, Funding acquisition, Investigation. **Michael Meyer:** IRSL dating, dosimetry and calculation of OSL ages, writing & reviewing. **Clemens Geitner:** Supervision, Conceptualization, Fieldwork, Resources, Reviewing. **Jean Nicolas Haas:** Palynological analyses, determination of snow algae and moss spores, Resources, Reviewing. **Sanja Vranjes-Wessely:** IRSL dating at site 2. **Clivia Hejny:** Supervision of X-ray diffraction analyses, Resources. **Werner Kofler:** Palynological preparations and analyses. **Karl Krainer:** Supervision of heavy mineral analyses. **Daniel Remias:** Determination of snow algae. **Sönke Szidat:** AMS radiocarbon analyses. **Diethard Sanders:** Supervision, Conceptualization, Fieldwork, Resources, Investigation, Writing – original draft, Writing – review & editing.

Declaration of competing interest

The authors declare that they have no known competing financial interests or personal relationships that could have appeared to influence the work presented in this paper.

Data availability

Data will be made available on request.

Acknowledgements

This paper is part of the PhD thesis of Charlotte Gild. Financial support from grant “Nachwuchsförderung der Universität Innsbruck” (fund 2014/3/GEO-8), and from grant "Äolische Sedimente in den Nördlichen Kalkalpen von Tirol als stratigraphische Zeitmarker im Quartär" (fund AP716031 LADS Tyrol) of the Tyrolean Science Fund, both donated to Charlotte Gild, is gratefully acknowledged. Daniel Remias acknowledges the Austrian Science Fund (FWF) P 34073 for funding. The XRF scanning data was acquired at the Austrian Core Facility, Institute of Geology, University of Innsbruck, and discussions of results with Michael Strasser, Jyh-Jaan Huang, and Marcel-Luciano Ortler are gratefully acknowledged. Taxonomic determinations of charcoal fragments were done by Werner Schoch, Laboratory for Ancient Wood Research, Langnau/Switzerland. Discussions with Michael Zech and Marcel Lerch, University of Dresden/Germany, as well as with Dieter Schäfer, University of Innsbruck, of the results obtained at site 2 are highly appreciated.

Appendix A. Supplementary data

Supplementary data to this article can be found online at https://doi.org/10.1016/j.quascirev.2024.108959.

References

Ahrens, M., 2000. Funariales. Funariaceae – drehmoose. In: Nebel, M., Philippi, G. (Eds.), Die Moose Baden-Württembergs. Band 1: Allgemeiner Teil. Spezieller Teil (Bryophytina I, Andreaeales Bis Funariales. Eugen Ulmer, Stuttgart, pp. 474–492.
Ammann, B., Birks, H.J.B., Brooks, S.J., Eicher, U., von Grafenstein, U., Hofmann, W., Lemdahl, G., Schwander, J., Tobolski, K., Wick, L., 2000. Quantification of biotic responses to rapid climatic changes around the Younger Dryas – a synthesis. Palaeogeogr. Palaeoclimatol. Palaeoecol. 159, 313–347.
Angelucci, D.E., Bassetti, M., 2009. Humans and their landscape from the alpine last glacial maximum to the middle Holocene in Trentino: geoarcheological considerations. Preistoria Alp. 44, 1–6.
Ashmore, P., 2022. Braiding. In: Wohl, E. (Ed.), Treatise on Geomorphology, vol. 6. Academic Press, Elsevier, pp. 517–543.
Balescu, S., Huot, S., Mejri, H., Barre, M., Forget Brisson, L., Lamothe, M., Oueslati, A., 2015. Luminescence dating of Middle Pleistocene (MIS 7) marine shoreline deposits along the eastern coast of Tunisia: a comparison of K-feldspar and Na-feldspar IRSL ages. Quat. Geochronol. 30 (Part B), 288–293.
Ballantyne, C.P., Brahney, J., Fernandez, D., et al., 2011. Biogeochemical response of alpine lakes to a recent increase in dust deposition in the southwestern, US. Biogeosciences 8, 2689–2706.
Baroni, C., Casale, S., Salvatore, M.C., Ivy-Ochs, S., Christl, M., Carturan, L., Seppi, R., Carton, A., 2017. Double response of glaciers in the upper Peio valley (Rhaetian Alps, Italy) to the Younger Dryas climatic deterioration. Boreas 46, 783–798.
Barré, M., Lamothe, M., 2010. Luminescence dating of archaeosediments: a comparison of K-feldspar and plagioclase IRSL ages. Quat. Geochronol. 5, 324–328.
Barrett, S., Starnberger, R., Tjallingii, R., Brauer, A., Spötl, C., 2017. The sedimentary history of the inner-alpine Inn Valley, Austria: extending the Baumkirchen type section further back in time with new drilling. J. Quat. Sci. 32, 63–79.
Bäumler, R., 2001. Pedogenic studies in aeolian deposits in the high mountain area of eastern Nepal. Quat. Int. 76 (/77), 93–102.
Bichler, M.G., Reindl, M., Reitner, J.M., Drescher-Schneider, R., Wirsig, C., Christl, M., Hajdas, I., Ivy-Ochs, S., 2016. Landslide deposits as stratigraphical markers for a sequence-based glacial stratigraphy: a case study of a Younger Dryas system in the Eastern Alps. Boreas 45, 537–551.
Bigelow, A., Mladenov, N., Lipson, D., Williams, M., 2020. Dust deposition drives microbial metabolism in a remote, high-elevation catchment. Holocene 30, 589–596.
Blaas, J., 1885. Ueber die Glacialformation im Innthale. Zeitschrift des Ferdinandeums für Tirol und Vorarlberg, 3. Folge, 29. Heft, 1—129.
Blockley, S.P.E., Lane, C.S., Hardiman, M., Rasmussen, S.O., Seierstad, I.K., Steffensen, J. P., Svensson, A., Lotter, A.F., Turney, C.S.M., Bronk Ramsey, C., INTIMATE Members, 2012. Synchronisation of palaeoenvironmental records over the last 60,000 years, and an extended INTIMATE event stratigraphy to 48,000 b2k. Quat. Sci. Rev. 36, 2–10.
Boch, R., Spötl, C., Kramers, J., 2009. High-resolution isotope records of early Holocene rapid climate change from two coeval stalagmites of Katerloch Cave, Austria. Quat. Sci. Rev. 28, 2527–2538.
Boenigk, W., 1983. Schwermineralanalyse. Ferdinand Enke Publishers, Stuttgart, p. 152.
Boros, A., Járai-Komlódi, M., Tóth, Z., Nilsson, S., 1993. An Atlas of Recent European Bryophyte Spores. Scientia Publishing, Budapest, Hungary, p. 321.
Bortenschlager, S., 1984a. Die Vegetationsentwicklung im Spätglazial: Das Moor beim Lanser See III. Ein Typprofil für die Ostalpen. Diss. Bot. 72, 71–79.
Bortenschlager, S., 1984b. Beiträge zur Vegetationsgeschichte Tirols. I. Inneres Ötztal und unteres Inntal. Berichte des naturwissenschaftlich-medizinischen Vereins Innsbruck 71, 19–56.
Bortenschlager, S., 1992. Die Waldgrenze im Postglazial. In: Eder-Kovar, J. (Ed.), Palaeovegetational Development in Europe and Regions Relevant to its Palaeofloristic Evolution, Proceedings of the Pan-European Palaeobotanical Conference in Vienna. Vienna, pp. 9–13.
Bos, J.A.A., van Geel, B., van der Plicht, J., Bohncke, S.J.P., 2007. Preboreal climate oscillations in Europe: wiggle-match dating and synthesis of Dutch high-resolution multi-proxy records. Quat. Sci. Rev. 26, 1927–1950.
Bøtter-Jensen, L., Mejdahl, V., 1988. Assessment of beta dose-rate using a GM multicounter system. Nuclear tracks and radiation measurements 14, 187–191.
Brauer, A., Haug, G.H., Dulski, P., Sigman, D.M., Negendank, J.F.W., 2008. An abrupt wind shift in western Europe at the onset of the Younger Dryas cold period. Nat. Geosci. 1, 520–523.
Bullard, J.E., Austin, M.J., 2011. Dust generation on a proglacial floodplain, West Greenland. Aeolian Research 3, 43–53.
Buylaert, J.P., Jain, M., Murray, A.S., Thomsen, K.J., Thiel, C., Sohbati, R., 2012. A robust feldspar luminescence dating method for Middle and Late Pleistocene sediments. Boreas 41, 435–451.
Cano, M.J., Ros, R.M., Guerra, J., Gonzales, J., 1999. The identity of *Entosthodon hungaricus* (boros) loeske and *E. maroccanus* (meyl.) hébr. & lo giudice (= *Physocomitrium maroccanum* meyl.). J. Bryolog. 21, 67–70.
Carcaillet, C., 2001. Are Holocene wood-charcoal fragments stratified in alpine and subalpine soils? Evidence from the Alps based on AMS ^{14}C dates. Holocene 11, 231–242.
Caspari, T., Bäumler, R., Norbu, C., Tshering, K., Baillie, I., 2009. Soil formation in Phobjikha Valley, Central Bhutan with special regard to the redistribution of loessic sediments. J. Asian Earth Sci. 34, 403–417.
Castiglioni, G.B., Cremaschi, M., Guerreschi, A., Meneghel, M., Sauro, U., Van Vliet Lanoe, B., 1990. The loess deposits in the Lessini plateau. In: Cremaschi, M. (Ed.), The Loess in Northern and Central Italy: A Loess Basin between the Alps and the Mediterranean Region, Centro di Studio per la Stratigrafia e Petrografia delle Alpi Centrali, vol. 1. Quaderni di Geodinamica Alpina e Quaternaria, pp. 41–59.
Cremaschi, M., 1990. The loess in northern and central Italy: a loess basin between the Alps and the Mediterranean regions. In: Cremaschi, M. (Ed.), The Loess in Northern and Central Italy: A Loess Basin between the Alps and the Mediterranean Region, Centro di Studio per la Stratigrafia e Petrografia delle Alpi Centrali, vol. 1. Quaderni di Geodinamica Alpina e Quaternaria, pp. 15–19.
David, B., Roberts, R.G., Magee, J., Mialanes, J., Turney, C., Bird, M., White, C., Fifield, L.K., Tibby, J., 2007. Sediment mixing at Nonda Rock: investigations of stratigraphic integrity at an early archaeological site in northern Australia and implications for the human colonisation of the continent. J. Quat. Sci. 22, 449–479.
Daxer, C., Moernaut, J., Taylor, T., Haas, J.N., Strasser, M., 2018. Late Glacial and Holocene sedimentary infill of lake Mondsee (Eastern Alps, Austria) and historical rockfall activity revealed by reflection seismics and sediment core analysis. Austrian Journal of Earth Sciences 111, 111–134.
DeLong, S.B., Arnold, L.J., 2007. Dating alluvial deposits with optically stimulated luminescence, AMS ^{14}C and cosmogenic techniques, western Transverse Ranges, California, USA. Quat. Geochronol. 2, 129–136.
Denton, G.H., Alley, R.B., Comer, G.C., Broecker, W.S., 2005. The role of seasonality in abrupt climate change. Quat. Sci. Rev. 24, 1159–1182.
Eagar, J.D., Herckes, P., Hartnett, H.E., 2017. The characterization of haboobs and the deposition of dust in Tempe, AZ from 2005 to 2014. Aeolian Research 24, 81–91.
Felber, M., Veronese, L., Cocco, S., Frei, W., Nardin, M., Oppizzi, P., Santuliana, E., Violanti, D., 2000. Indagini sismiche geognostiche nelle valli del Trentino meridionale (Val d’Adige, Valsugana, Valle del Sarca, Valle del Chiese). Studi Trentini di Scienze Naturale. Acta Geol. 75, 3–52.
Fenn, K., Millar, I.L., Durcan, J.A., Thomas, D.S.G., Banak, A., Markovic, S.B., Veres, D., Stevens, T., 2022. The provenance of Danubian loess. Earth Sci. Rev. 226, 103920.
Fink, J., Kukla, G.J., 1977. Pleistocene climates in central Europe: at least 17 interglacials after the Olduvai event. Quaternary Research 7, 363–371.
Fisher, T.G., Smith, D.G., Andrews, J.T., 2002. Preboreal oscillation caused by a glacial lake agassiz flood. Quat. Sci. Rev. 21, 873–878.
Forno, M.G., 1979. Il loess della Collina di Torino: revisione della sua distribuzione e della sua interpretazione genetica e morfologica. Geogr. Fis. Din. Quaternaria 2, 105–124.
Fraedrich, R., 1975. Spät- und postglaziale Gletscherschwankungen in der Verwallgruppe (Tirol/Vorarlberg). Dusseld. Geogr. Schriften 12, 1–161.
Frechen, M., Oches, E.A., Kohfeld, K.E., 2003. Loess in europe–mass accumulation rates during the last glacial period. Quat. Sci. Rev. 22, 1835–1857.
French, H.M., 2007. The Periglacial Environment, third ed. John Wiley & Sons Ltd., Chicester, p. 458.
Fuganti, A., Bazzoli, G., Morteani, G., 1998. The Quaternary evolution of the Adige Valley near the city of Trento (Northern Italy) as deduced from wells and radiocarbon dating. Preliminary results. Studi Trentini di Scienze Naturale. Acta Geol. 73, 93–98.
Geilhausen, M., Otto, J.C., Schrott, L., 2012. Spatial distribution of sediment storage types in two glacier landsystems (Pasterze und Obersulzbachkees, Hohe Tauern, Austria). J. Maps 8, 242–259.
Geitner, C., Bussemer, S., Ehrmann, O., Ikinger, A., Schäfer, D., Traidl, R., Tscherko, D., 2011. Bodenkundlich-stratigraphische Befunde am Ullafelsen im hinteren

Fotschertal sowie ihre landschaftsgeschichtliche Interpretation. In: Schäfer, D. (Ed.), Das Mesolithikum-Projekt Ullafelsen (Teil 1), Mensch und Umwelt im Holozän Tirols, Band 1. Verlag Philip von Zabern GmbH, Darmstadt, pp. 109–151.
Geitner, C., Schäfer, D., Bertola, S., Bussemer, S., Heinrich, K., Waroszewski, J., 2014. Landscape archaeological results and discussion of Mesolithic research in the Fotsch valley (Tyrol). In: Kerschner, H., Krainer, K., Spötl, C. (Eds.), From the Foreland to the Central Alps. Field Trips to Selected Sites of Quaternary Research in the Tyrolean and Bavarian Alps. Geozon Science Media, Berlin, pp. 108–117.
Gild, C., Geitner, C., Sanders, D., 2018. Discovery of a landscape-wide drape of Late Glacial aeolian silt in the western Northern Calcareous Alps (Austria): first results and implications. Geomorphology 301, 39–52.
Good, T.R., Bryant, I.D., 1985. Fluvio-aeolian sedimentation: an example from banks island, N.W.T., Canada. Geografiska annaler, series A. Phys. Geogr. 67, 33–46.
Grashey-Jansen, S., Korch, O., Beck, C., Friedmann, A., Bernhard, R., Dubitzky, C., 2014. Aeolian influenced soil sites in condsideration of atmospheric circulation types – a case study in the alpine zone of the Zugspitzplatt (Northern Calcareous Alps, Germany). International Journal of Geology, Agriculture and Environmental Sciences 2, 11–19.
Grüger, E., Jerz, H., 2010. Untersuchung einer Doline auf dem Zugspitzplatt. E&G Quaternary Science Journal 59, 66–75.
Guerin, G., Mercier, N., 2011. Determining gamma dose rates by field gamma spectroscopy in sedimentary media: results of Monte Carlo simulations. Radiat. Meas. 46, 190–195.
Hales, T.C., Roering, J.J., 2009. A frost "buzzsaw" mechanism for erosion of the eastern Southern Aps, New Zealand. Geomorphology 107, 241–253.
Hallet, B., Hunter, L., Bogen, J., 1996. Rates of erosion and sediment evacuation by glaciers: a review of field data and their implications. Global Planet. Change 12, 213–235.
Hammer, W., 1929. Geologische Spezialkarte der Republik Österreich 1:75.000, 5146 Ötzthal. Geologische Bundesanstalt, Wien.
Handy, M.R., Ustaszewski, K., Kissling, E., 2015. Reconstructing the Alps-Carpathians–Dinarides as a key to understanding switches in subduction polarity, slab gaps and surface motion. Int. J. Earth Sci. 104, 1–26.
Hao, Y., Han, Y., Shu, P., Zhao, J., Zhang, Z., An, Z., 2023. Holocene wildfire on the Quinghai-Tibetan plateau – witness of abrupt millennial timescale climate events. Quat. Sci. Rev. 321, 108373.
Heiri, O., Koinig, K.A., Spötl, C., 16 coauthors, 2014. Paleoclimate records 60-8 ka in the Austrian and Swiss Alps and their forelands. Quat. Sci. Rev. 106, 186–205.
Heller, F., Liu, T.-S., 1982. Magnetostratigraphical dating of loess deposits in China. Nature 300, 431–433.
Henderson, G.M., 2006. Caving into new chronologies. Science 313, 620–622.
Hodell, D.A., Nicholl, J.A., Bontognali, T.R.R., Danino, S., Dorador, J., Dowdeswell, J.A., Einsele, J., Kuhlmann, H., Martrat, B., Mleneck-Vautravers, M.J., Rodríguez-Tovar, F.J., Röhl, U., 2017. Anatomy of Heinrich Layer 1 and its role in the last deglaciation. Paleoceanogr. Paleoclimatol. 32, 284–303.
Hoham, R.W., Remias, D., 2020. Snow and glacial algae: a review. J. Phycol. 56, 264–282.
Hugenholtz, C.H., Wolfe, S.A., 2010. Rates and environmental controls of aeolian dust accumulation, athabasca river valley, Canadian rocky mountains. Geomorphology 121, 274–282.
Huntley, D.J., Baril, M.R., Haidar, S., 2007. Tunnelling in plagioclase feldspars. Journal of Physics D, Applied Physics 40, 900–906.
Ilyashuk, B., Gobet, E., Heiri, O., Lotter, A.F., van Leeuwen, J.F.N., van der Knaap, W.O., Ilyashuk, E., Oberli, F., Ammann, B., 2009. Lateglacial environmental and climatic changes at the Maloja Pass, Central Swiss Alps, as recorded by chironomids and pollen. Quat. Sci. Rev. 28, 1340–1353.
Ivy-Ochs, S., 2015. Glacier variations in the European Alps at the end of the last glaciation. Cuadernos de Investigación Geográfica 41, 295–315.
Ivy-Ochs, S., Kerschner, H., Kubik, P., Schlüchter, C., 2005. Glacier response in the European Alps to Heinrich event 1 cooling: the Gschnitz stadial. J. Quat. Sci. 20, 1–16.
Ivy-Ochs, S., Kerschner, H., Reuther, A., Sailer, R., Schaefer, J., Kubik, P.W., Synal, H.-A., Schlüchter, C., 2006. The timing of glacier advances in the northern European Alps based on surface exposure dating with cosmogenic ^{10}Be, ^{26}Al, ^{36}Cl, and ^{21}Ne. Geol. Soc. Am. Spec. Pap. 415, 43–60.
Ivy-Ochs, S., Kerschner, H., Reuther, A., Preusser, F., Heine, K., Maisch, M., Kubik, W.P., Schlüchter, C., 2008. Chronology of the last glacial cycle in the European Alps. J. Quat. Sci. 23, 559–573.
Ivy-Ochs, S., Kerschner, H., Maisch, M., Christl, M., Kubik, P.W., Schlüchter, C., 2009. Latest Pleistocene and Holocene glacier variations in the European Alps. Quat. Sci. Rev. 28, 2137–2149.
Kerschner, H., 2011. Spätglaziale Gletschervorstöße im Fotschertal. In: Schäfer, D. (Ed.), Das Mesolithikum-Projekt Ullafelsen (Teil 1), Mensch und Umwelt im Holozän Tirols, Band 1. Verlag Philip von Zabern GmbH, Darmstadt, pp. 95–103.
Kerschner, H., Ivy-Ochs, S., 2008. Palaeoclimate from glaciers: examples from the eastern Alps during the alpine lateglacial and early Holocene. Global Planet. Change 60, 58–71.
Kerschner, H., Kaser, G., Sailer, R., 2000. Alpine Younger Dryas glaciers as palaeo-precipitation gauges. Ann. Glaciol. 31, 80–84.
Klinge, M., Lehmkuhl, F., 2015. Holocene aeolian mantles and inter-bedded paleosols on the southern Tibetan Plateau. Quat. Int. 372, 33–44.
Knippertz, P., Stuut, J.-B., 2014. Mineral Dust: A Key Player in the Earth System. Springer, New York, p. 509.
Kohfeld, K.E., Harrison, S.P., 2001. DIRTMAP: the geological record of dust. Earth Sci. Rev. 54, 81–114.
Kol, E., 1968. Kryobiologie. Biologie und Limnologie des Schnees und Eises. I. Kryovegetation. E. Schweizerbart'sche Verlagsbuchhandlung, Stuttgart, p. 216.
Koltai, G., Cheng, H., Spötl, C., 2018. Palaeoclimate significance of speleothems in crystalline rocks: a test case from the Late Glacial and early Holocene (Vinschgau, northern Italy). Clim. Past 14, 369–381.
Koltai, G., Spötl, C., Cheng, H., 2021. Cryogenic cave carbonates in the Dolomites (Northern Italy): insights into Younger Dryas cooling and seasonal precipitation. Clim. Past 17, 775–789.
Krainer, K., Bressan, D., Dietre, B., Haas, J.N., Hajdas, I., Lang, K., Mair, V., Nickus, U., Reidl, D., Thies, H., 2015. A 10,300-year-old permafrost core from the active rock glacier Lazaun, southern Oetztal Alps (South Tyrol, northern Italy). Quaternary Research 83, 324–335.
Kravogl, H., 1873. Zusammensetzung und Lagerung des Diluviums um Innsbruck. Ber. Natwiss.-Med. Ver. Innsbr. 3, 74–86.
Küfmann, C., 2003. Soil types and eolian dust in high-mountainous karst of the northern calcareous Alps (Zugspitzplatt, wetterstein mountains, Germany). Catena 53, 211–227.
Küfmann, C., 2008. Are Cambisols in Alpine karst autochthonous or eolian in origin? Arctic Antarct. Alpine Res. 40, 506–518.
Langford, R.P., 1989. Fluvial-aeolian interactions: Part I, modern systems. Sedimentology 36, 1023–1035.
Larsen, A., Bork, H.-R., Fuelling, A., Fuchs, M., Larsen, J.R., 2013. The processes and timing of sediment delivery from headwaters to the trunk stream of a Central European mountain gully catchment. Geomorphology 201, 215–226.
Latrubesse, E.M., Stevaux, J.C., Cremon, E.H., May, J.-H., Tatumi, S.H., Hurtado, M.A., Bezada, M., Argollo, J.B., 2012. Late quaternary megafans, fans and fluvio-aeolian interactions in the Bolivian chaco, tropical south America. Palaeogeogr. Palaeoclimatol. Palaeoecol. 356–357, 75–88.
Lauterbach, S., Brauer, A., Andersen, N., Danielopol, D.L., Dulski, P., Hüls, M., Milecka, K., Namiotko, T., Obremska, M., Von Grafenstein, U., Declakes, Participants, 2011. Environmental responses to Lateglacial climatic fluctuations recorded in the sediments of pre-Alpine Lake Mondsee (northeastern Alps). J. Quat. Sci. 26, 253–267.
Lawrence, C.R., Neff, J.C., Farmer, G.L., 2011. The accretion of aeolian dust in soils of the San Juan Mountains, Colorado, USA. J. Geophys. Res. 116, F02013.
Lehmkuhl, F., Klinge, M., Rees-Jones, J., Rhodes, E.J., 2000. Late Quaternary aeolian sedimentation in central and south-eastern Tibet. Quat. Int. 68–71, 117–132.
Li, Y., Shi, W., Aydin, A., Beroya-Eitner, M.A., Gao, G., 2020. Loess genesis and worldwide distribution. Earth Sci. Rev. 201, 102947.
Li, H., Spötl, C., Cheng, H., 2021. A high-resolution speleothem proxy record of the Late Glacial in the European Alps: extending the NALPS19 record until the beginning of the Holocene. J. Quat. Sci. 36 (1), 29–39.
Lieb, G.K., Kellerer-Pirklbauer, A., 2022. Großglockner and Pasterze Glacier: landscape evolution at Austria's highest summit and its neighbouring glacier system. In: Landscapes and Landforms of Austria. Springer International Publishings, Cham, pp. 367–378.
Liu, T.-S., 1965. The Loess Deposits in China. Science Press, Beijing, p. 224 (In Chinese).
Liu, T.-S. (Ed.), 1985. Loess and the Environment. China Ocean Press, Beijing, p. 251.
Lotter, A.F., Birks, H.J.B., Eicher, U., Hofmann, W., Schwander, J., Wick, L., 2000. Younger Dryas and Allerød summer temperatures at Gerzensee (Switzerland) inferred from fossil pollen and cladoceran assemblages. Palaeogeogr. Palaeoclimatol. Palaeoecol. 159, 349–361.
Mange, M.A., Maurer, H.F.W., 1992. Heavy Minerals in Colour. Chapman and Hall, London, p. 147.
Martignier, L., Nussbaumer, M., Adatte, T., Gobat, J.M., Verrecchia, E.P., 2015. Assessment of a locally-sourced loess system in Europe: the Swiss jura mountains. Aeolian Research 18, 11–21.
McGowan, H.A., 1997. Meteorological controls on wind erosion during foehn wind events in the easter Southern Alps, New Zealand. Can. J. Earth Sci. 34, 1477–1485.
McGowan, H.A., Sturman, A.P., 1997. Characteristics of aeolian grain transport over a fluvio-glacial lacustrine braid delta, Lake Tekapo, New Zealand. Earth Surf. Process. Landforms 22, 773–784.
Megies, H., 2006. Kartierung, Datierung und umweltgeschichtliche Bedeutung der jungquartären Flussterrassen am unteren Inn. In: Heidelberger Geographische Arbeiten, vol. 120. Institute of Geography, University of Heidelberg, Heidelberg, p. 206.
Meyer, M.C., Spötl, C., Mangini, A., Tessadri, R., 2012. Speleothem deposition at the glaciation threshold—an attempt to constrain the age and paleoenvironmental significance of a detrital-rich flowstone sequence from Entrische Kirche Cave (Austria). Palaeogeogr. Palaeoclimatol. Palaeoecol. 319, 93–106.
Moran, A.P., Ivy-Ochs, S., Schuh, M., Christl, M., Kerschner, H., 2016a. Evidence of central Alpine glacier advances during the Younger Dryas-early Holocene transition period. Boreas 45, 398–410.
Moran, A.P., Ivy-Ochs, S., Vockenhuber, C., Kerschner, H., 2016b. Rock glacier development in the northern calcareous Alps at the pleistocene-holocene boundary. Geomorphology 273, 178–188.
Muhs, D.R., 2013. The geologic records of dust in the Quaternary. Aeolian Research 9, 3–48.
Muhs, D.R., Benedict, J.B., 2006. Eolian additions to late quaternary alpine soils, Indian peaks wilderness area, Colorado front range. Arctic Antarct. Alpine Res. 38, 120–130.
Muhs, D.R., Budahn, J.R., McGeehin, J.P., Bettis III, E.A., Skipp, G., Paces, J.B., Wheeler, E.A., 2013. Loess origin, transport, and deposition over the past 10,000 years, wrangell-St.Elias national park, Alaska. Aeolian Research 11, 85–99.
Munroe, J.S., Attwood, E.C., O'Keefe, S.S., Quackenbush, P.J.M., 2015. Eolian deposition in the alpine zone of the Uinta Mountains, Utah, USA. Catena 124, 119–129.

Munroe, J.S., Norris, E.D., Olson, P.M., Ryan, P.C., Tappa, M.J., Beard, B.L., 2020. Quantifying the contribution of dust to alpine soils in the periglacial zone of the Uinta Mountains, Utah, USA. Geoderma 378, 114631.
Murray, A.S., Wintle, A.G., 2000. Luminescence dating of quartz using an improved single-aliquot regenerative-dose protocol. Radiation measurement 32, 57–73.
Murton, J.B., Peterson, R., Ozouf, J.-C., 2006. Bedrock fracture by ice segregation in cold regions. Science 314, 1127–1129.
Nickling, W.G., 1983. Grain-size characteristics of sediment transported during dust storms. J. Sediment. Petrol. 53, 1011–1024.
Nigst, P.R., Haesaerts, P., Damblonc, F., Frank-Fellnerd, C., Mallole, C., Viola, B., Götzinger, M., Nivena, L., Trnka, G., Hublin, J.J., 2014. Early modern human settlement of Europe north of the Alps occurred 43,500 years ago in a cold steppe-type environment. Proceedings of the National Academy of Sciences of the United States of America 111, 14394–14399.
Nittel, P., 2011. Geologie, Hydrogeologie und Geomorphologie des Fotschertales – Kartierungsergebnisse Projekt "Sellrain" 2006. In: Schäfer, D. (Ed.), Das Mesolithikum-Projekt Ullafelsen (Teil 1). Mensch und Umwelt im Holozän Tirols, Band 1. Verlag Philipp von Zabern, GmbH, Darmstadt, pp. 61–92.
Oberhauser, R., 1980. Der Geologische Aufbau Osterreichs. Springer, New York, p. 700.
Oerlemans, J., 2005. Extracting a climate signal from 169 glacier records. Science 308, 675–677.
Patzelt, G., 1987. Untersuchungen zur nacheiszeitlichen Schwemmkegel- und Talentwicklung in Tirol. Veröffentlichungen des Tiroler Landesmuseums Ferdinandeum 67, 93–123.
Patzelt, G., 2014. Das Mammutzahn-Bruchstück von Fritzens (Inntal, Tirol) und seine Stellung in der Chronologie des ostalpinen Spätpleistozäns. Jahrbuch der geologischen Bundesanstalt 154, 71–82.
Patzelt, G., Resch, W., 1986. Quartärgeologie des mittleren Tiroler Inntales zwischen Innsbruck und Baumkirchen. Jahresberichte und Mitteilungen des oberrheinischen geologischen Vereins. Neue Folge 68, 43–66.
Patzelt, G., Weber, A., 2015. Die nacheiszeitliche Entwicklung des Schwemmfächers von Kundl und des Talraumes im Inntal (Tirol). Jahrbuch der geologischen Bundesanstalt 155, 11–31.
Peer, T., Zheng, L.J., Neubauer, F., Friedl, G., Hauzenberger, C., Kasper-Giebl, A., 2022. Mineralogical composition and origin of airborne dust in an alpine environment of Hochtor (Hohe Tauern, Austria): effects on pedogenesis, biological soil crusts, and vascular plant growth. Front. Earth Sci. 10, 871211.
Reimer, P.J., Austin, W.E.N., Bard, E., 39 coauthors, 2020. The IntCal20 Northern Hemisphere radiocarbon age calibration curve (0-55 cal kBP). Radiocarbon 62, 725–757.
Reinig, F., Wacker, L., Jöris, O., Oppenheimer, C., Guidobaldi, G., Nievergelt, D., Adolphi, F., Cherubini, P., Engels, S., Esper, J., Land, A., Lane, C., Pfanz, H., Remmele, S., Sigl, M., Sookdeo, A., Büntgen, U., 2021. Precise date for the laacher see eruption synchronizes the younger Dryas. Nature 595, 66–69.
Rey, F., Schwörer, C., Gobet, E., Colombaroli, D., van Leeuwen, J.F.N., Schleiss, S., Tinner, W., 2013. Climatic and human impacts on vegetation at Lauensee (Bernese Alps, Switzerland) during the last 14,000 years. Holocene 23, 1415–1427.
Reynolds, R., Belnap, J., Reheis, M., Lamothe, P., Luiszer, F., 2001. Aeolian dust in Colorado Plateau soils: nutrient inputs and recent change in source. Proceedings of the National Academy of Science 98, 7123–7127.
Roberts, H.M., Muhs, D.R., Wintle, A.G., Duller, G.A.T., Bettis III, E.A., 2003. Unprecetended last-glacial mass accumulation rates determined by luminescence dating of loess from western Nebraska. Quaternary Research 59, 411–419.
Sanders, D., Pomella, H., Gild, C., 2018. Early late-glacial rock avalanche and its lasting effects on drainage and sediment dispersal (Strassberg valley catchment, Northern Calcareous Alps, Austria). Austrian Journal of Earth Sciences 111 (2), 180–203.
Sass, O., Wetzel, K.-F., Friedmann, A., 2006. Landscape dynamics of sub-alpine forest fire slopes in the Northern Alps. Zeitschrift für Geomorphologie, Supplement 142, 207–227.
Schaetzl, R.J., Nyland, K.E., Kasmerchak, C.S., Breeze, V., Kamoske, A., Thomas, S.E., Bomber, M., Grove, L., Komoto, K., Miller, B.A., 2021. Holocene, silty-sand loess downwind of dunes in Northern Michigan, USA. Phys. Geogr. 42, 25–49.
Schäfer, D., 2011a. Zum aktuellen Stand des 'Mittelsteinzeit-Projektes Ullafelsen' (2010). In: Schäfer, D. (Ed.), Das Mesolithikum-Projekt Ullafelsen (Teil 1). Mensch und Umwelt im Holozän Tirols, Band 1. Verlag Philipp von Zabern, GmbH, Darmstadt, pp. 547–552.
Schäfer, D., 2011b. Das Mesolithikum-Projekt Ullafelsen – Landschaftlicher Rahmen und archäologische Befunde. In: Schäfer, D. (Ed.), Das Mesolithikum-Projekt Ullafelsen (Teil 1). Mensch und Umwelt im Holozän Tirols, Band 1. Verlag Philipp von Zabern, GmbH, Darmstadt, pp. 245–351.
Schäfer, D., Bertola, S., Pawlik, A., Geitner, C., Warozewksi, J., Bussemer, S., 2016. The landscape-archaeological ullafelsen project (Tyrol, Austria). Preistoria Alp. 48, 33–41.
Schneider, H., Höfer, D., Irmler, R., Daut, G., Mäusbacher, R., 2010. Correlation between climate, man and debris flow events – a palynological approach. Geomorphology 120, 48–55.
Seiwald, A., 1980. Beiträge zur Vegetationsgeschichte Tirols IV: Natzer Plateau – Villanderer Alm. Berichte des naturwissenschaftlich-medizinischen Vereins in Innsbruck 67, 31–72.
Shao, Y., Wyrwoll, K.-H., Chappell, A., Huang, J., Lin, Z., McTainsh, G.H., Mikami, M., Tanaka, T.Y., Wang, X., Yoon, S., 2011. Dust cycle: an emerging core theme in Earth system science. Aeolian Research 2, 181–204.
Smalley, I., O'Hara-Dhand, K., Wint, J., Machalett, B., Jary, Z., Jefferson, I., 2009. Rivers and loess: the significance of long river transportation in the complex event-sequence approach to loess deposit formation. Quat. Int. 198, 7–18.
Sohbati, R., Murray, A.S., Jain, M., Thomsen, K.J., Hong, S.-C., Yi, K., Choi, J.-H., 2013. Na-rich feldspar as a luminescence dosimeter in infrared stimulated luminescence (IRSL) dating. Radiation Measurement 51–52, 67–82.
Spötl, C., Reimer, P.J., Starnberger, R., Reimer, R.W., 2014. A new radiocarbon chronology of Baumkirchen, stratotype for the onset of the Upper Würmian in the Alps. J. Quat. Sci. 28, 552–558.
Starnberger, R., Drescher-Schneider, R., Reitner, J.M., Rodnight, H., Reimer, P., Spötl, C., 2013. Late Pleistocene climate change and landscape dynamics in the Eastern Alps: the inner-alpine Unterangerberg record (Austria). Quat. Sci. Rev. 68, 17–42.
Steinemann, O., Reitner, J., Ivy-Ochs, S., Christl, M., Synal, H.-A., 2020. Tracking rockglacier evolution in the eastern Alps from the lateglacial to the early Holocene. Quat. Sci. Rev. 241, 106424.
Stevens, T., Buylaert, J.P., Thiel, C., Újvári, G., Yi, S., Murray, A.S., Frechen, M., Lu, H., 2018. Ice-volume-forced erosion of the Chinese Loess Plateau global Quaternary stratotype site. Nat. Commun. 9, 1–12.
Sticher, H., Bach, R., Brugger, H., Vökt, U., 1975. Flugstaub in vier Böden aus Kalk, Dolomit und Serpentin (Schweizer Jura und Schweizer Alpen). Catena 2, 11–22.
Stockmarr, J., 1971. Tables with spores used in absolute pollen analysis. Pollen Spores 13, 615–621.
Stoops, G., 2003. Guidelines for Analysis and Description of Soil and Rhegolith Thin Sections. Soil Science Society of America, Inc., Madison, USA, p. 184.
Stoops, G., Marcelino, V., Mees, F., 2010. Micromorphological features and their relation to processes and classification: general guidelines and keys. In: Interpretation of Micromorphological Features of Soils and Rhegoliths, pp. 15–108.
Szidat, S., Salazar, G.A., Vogel, E., Battaglia, M., Wacker, L., Synal, H.-A., Türler, A., 2014. ^{14}C analysis and sample preparation at the new Bern Laboratory for the Analysis of Radiocarbon with AMS (LARA). Radiocarbon 56, 561–566.
Terhorst, B., Frechen, M., Reitner, J., 2002. Chronostratigraphische Ergebnisse aus Lößprofilen der Inn- und Traunhochterrasse in Oberösterreich. Zeitschrift für Geomorphologie, Neue Folge, Supplement-Band 127, 213–232.
Terhorst, B., Kühn, P., Damm, B., Hambach, U., Meyer-Heintze, S., Sedov, S., 2014. Paleoenvironmental fluctuations as recorded in the loess-paleosol sequence of the Upper Paleolithic site Krems-Wachtberg. Quat. Int. 351, 67–82.
Thiel, C., Buylaert, J.-P., Murray, A.S., Terhorst, B., Tsukamoto, S., Frechen, M., 2011. Investigating the Chronostratigraphy of Prominent Palaeosols in Lower Austria using post-IR IRSL dating. E&G Quat. Sci. J. 60, 137–152.
Thomsen, K.J., Murray, A.S., Jain, M., Bøtter-Jensen, L., 2008. Laboratory fading rates of various luminescence signals from feldspar-rich sediment extracts. Radiat. Meas. 43, 1474–1486.
Tobolski, K., Ammann, B., 2000. Macrofossils as records of plant responses to rapid Late Glacial climatic changes at the three sites in the Swiss Alps. Palaeogeogr. Palaeoclimatol. Palaeoecol. 159, 251–259.
Töchterle, P., Baldo, A., Murton, J.B., Schenk, F., Edwards, R.L., Koltai, G., Moseley, G.E., 2023. Reconstructing Younger Dryas ground temperature and snow thickness from cave deposits. Clim. Past Discuss 2023, 1–21.
Újvári, G., Stevens, T., Molnár, M., Demény, A., Lambert, F., Varga, G., Jull, A.T., Páll-Gergely, B., Buylaert, J.P., Kovács, J., 2017. Coupled European and Greenland Last Glacial Dust Activity Driven by North Atlantic Climate, vol. 114. Proceedings of the National Academy of Sciences, pp. E10632–E10638.
Van Husen, D., 2000. Geological processes during the quaternary. Mittl. Osterreichischen Geol. Ges. 92, 135–156.
Van Husen, D., Reitner, J., 2011. An outline of the quaternary stratigraphy of Austria. Quaternary Science Journal (Eiszeitalter und Gegenwart) 60, 366–387.
Vandenberghe, J., 2003. Climate forcing of fluvial system development: an evolution of ideas. Quat. Sci. Rev. 22, 2053–2060.
Vandenberghe, J., Sun, Y., Wang, X., Abels, H.A., Liu, X., 2018. Grain-size characterization of reworked fine-grained aeolian deposits. Earth Sci. Rev. 177, 43–52.
Veit, H., Mailänder, R., Vonlanthen, C., 2002. Periglaziale Deckschichten im Alpenraum: bodenkundliche und landschaftsgeschichtliche Bedeutung. Petermanns Geogr. Mittl. 146, 6–14.
Ventra, D., Chong Dìaz, G., De Boer, P.L., 2013. Colluvial sedimentation in a hyperarid setting (Atacama Desert, northern Chile). Geomorphic controls and stratigraphic facies variability. Sedimentology 60, 1257–1290.
Vescovi, E., Ravazzi, C., Arpenti, E., Finsinger, W., Pini, R., Valsecchi, V., Wick, L., Ammann, B., Tinner, W., 2007. Interactions between climate and vegetation during the Lateglacial period as recorded by lake and mire sediment archives in Northern Italy and Southern Switzerland. Quat. Sci. Rev. 26, 1650–1669.
Wagenbrenner, N.S., Germino, M.J., Lamb, B.K., Robichaud, P.R., Foltz, R.B., 2013. Wind erosion from a sagebrush steppe burned by wildfire: measurements of PM_{10} and total horizontal sediment flux. Aeolian Research 10, 25–36.
Wentworth, C.K., 1922. A scale of grade and class terms for clastic sediments. J. Geol. 30, 377–392.
Wintle, A.G., 1997. Luminescence dating: laboratory procedures and protocols. Radiat. Meas. 27, 769–817.
Wolfe, S.A., Lian, O.B., 2021. Timing, rates and geomorphic controls on Holocene loess and aeolian sand deposition using multiple chronometric methods, southeastern Cordillera, Alberta, Canada. Aeolian Research 50, 100687.
Wurth, G., Niggemann, S., Richter, D.K., Mangini, A., 2004. The younger Dryas and Holocene climate record of a stalagmite from hölloch cave (bavarian Alps, Germany). J. Quat. Sci. 19, 291–298.
Yan, Y., Xu, X., Xin, X., Yang, G., Wang, X., Yan, R., Chen, B., 2011. Effect of vegetation coverage on aeolian dust accumulation in a semiarid steppe of northern China. Catena 87, 351–356.
Zárate, M.A., 2003. Loess of southern south America. Quat. Sci. Rev. 22, 1987–2006.

Zech, M., Lerch, M., Bliedtner, M., Bromm, T., Seemann, F., Szidat, S., Salazar, G., Zech, R., Glaser, B., Haas, J.N., Schäfer, D., Geitner, C., 2021. Revisiting the subalpine Mesolithic site Ullafelsen in the Fotsch valley, Stubai Alps, Austria – new insights into pedogenesis and landscape evolution from leaf-wax-derived *n*-alkanes, black carbon and radiocarbon dating. E&G Quaternary Science Journal 70, 171–186.

Zhang, J., Feng, J.-L., Hu, G., Wang, J., Yang, Y., Lin, Y., Jiang, T., Zhu, L., 2015. Holocene proglacial loess in the Ranwu valley, southeastern Tibet, and its paleoclimatic implications. Quat. Int. 372, 9–22.

Zhao, S., Xia, D., Lü, K., 2022. Holocene aeolian dust accumulation rates across the Chinese Loess Plateau. Global Planet. Change 208 (2022), 103720.